MAGNETIC HYPERFINE INTERACTIONS IN Sm^{149} IN FERROMAGNETIC $SmAl_2$

Thesis by
Arnold Vincent Lesikar

In Partial Fulfillment of the Requirements
For the Degree of
Doctor of Philosophy

California Institute of Technology
Pasadena, California
1965
(Submitted May 25, 1965)

ACKNOWLEDGEMENTS

Many people have contributed to the progress of this study. In particular the author would like to thank:

Dr. Rudolf Mössbauer, who suggested the study of recoilless gamma resonance in the isotope employed in this work and to whom the author is indebted for his invaluable guidance, counsel, and interest.

Professor Felix Boehm for his interest and support of these studies.

Dr. Egbert Kankeleit for indispensable aid and advice in the experiments, and in particular for the design and construction of the transducer drive and associated equipment.

Mr. Herbert E. Henderson, whose ingenuity and skill in the design of experimental equipment has been of enormous aid.

Mr. C. C. Chao for the preparation of the samarium alloy used in this work.

Mr. Frank T. Snively and Mr. Milton J. Clauser for instruction and advice in the use of the cryogenic equipment.

Mr. Richard Brockmeier for the least-squares fitting program used in the analysis of the experimental data and for advice in digital computer techniques.

Dr. Ulrich Hauser for his early encouragement.

This work was supported in part by the U. S. Atomic Energy Commission.

ABSTRACT

The internal field acting at the samarium nucleus in $SmAl_2$ is investigated theoretically and experimentally. The internal field is computed in the molecular field approximation assuming a crystalline electric field to act on the trivalent samarium ion. Admixtures of the first excited multiplet of the ion by the exchange and crystalline electric field are included in the calculation and lead to an increase of no more than 10% in the theoretically predicted internal field from the values predicted when the admixture is neglected if a crystal field interaction of reasonable size is assumed. The internal field resulting from theory is compared with the values resulting from Mössbauer studies of the hyperfine structure of the 22 kev gamma transition in Sm^{149}. The best fit made to the experimentally observed Mössbauer absorption patterns leads to an internal field much smaller than that predicted by theory. Possible sources of this disagreement between theory and experiment are discussed.

TABLE OF CONTENTS

I. INTRODUCTION

The elements of the rare earth series have long been of physical and chemical interest. These elements are characterized by a partially filled 4f shell lying deep inside the ion core and well-shielded from external influences. Many striking properties arise from this deeply buried 4f shell. Of the elements of the rare earth series samarium is of particular interest because in contrast to most of the other rare earths, its properties are strongly influenced by multiplet admixtures due to the unusually small spacing[1, 2] between the free ion electronic levels.

The present study is an investigation of the crystalline electric field and exchange interactions of samarium in $SmAl_2$ by means of recoilless nuclear gamma resonance measurements of the hyperfine interactions in Sm^{149}.

A quantity of major experimental concern in the study of magnetically ordered materials is the saturation magnetization. Related to this is the nuclear hyperfine magnetic field ("internal field"). These two quantities are usually related by a temperature independent constant of proportionality in the rare earth region. This is not so in samarium. The mixing of the low-lying first excited state in the samarium ion affects these two quantities quite differently[3].

A number of techniques are available for the study of the ionic magnetic moment or internal field in materials capable of magnetic ordering, such as neutron diffraction, ferromagnetic resonance, nuclear magnetic resonance, bulk magnetization or susceptibility measurements, and recoilless nuclear resonance (the Mossbauer effect). These techniques are complementary in their advantages

and disadvantages and in the information they secure. The Mossbauer effect, unlike the techniques requiring high frequency radio fields, is not limited by considerations of skin depth to the use of thin films in the study of conducting samples. Polycrystalline samples may be used in many measurements with the Mossbauer effect. Moreover, unlike the case of bulk measurements of magnetization or susceptibility, it is possible to study the ions of different elements separately, even in a complex substance containing several magnetic species. Furthermore, it is not necessary to magnetically saturate the sample with a large external magnetic field, and measurements with the Mossbauer effect may be carried out even in the case of very hard ferromagnets or substances of a complex spin configuration. For these reasons we have chosen the Mossbauer effect for this study.

Samarium offers a particularly favorable case for the use of the Mossbauer effect in magnetic studies, as there exists a gamma transition of 22.5 kev leading to the ground state of the stable isotope Sm^{149} (Figure I). This low transition energy gives a fairly large Debye-Waller factor (recoilless fraction) in most substances of interest, permitting measurements up to room temperature.

A number of magnetic samarium containing materials might have been chosen for this study. In order to simplify the interpretation of experimental data, we tried to choose a substance of as high a symmetry as possible at the samarium site and in which the only magnetically active ion is the samarium ion itself. A number of such compounds are available in the cubic Laves phase alloys[4]. In this case, according to the parameterization scheme previously applied by other workers, the high local symmetry of the samarium ion site reduces the number of parameters determining the pertur-

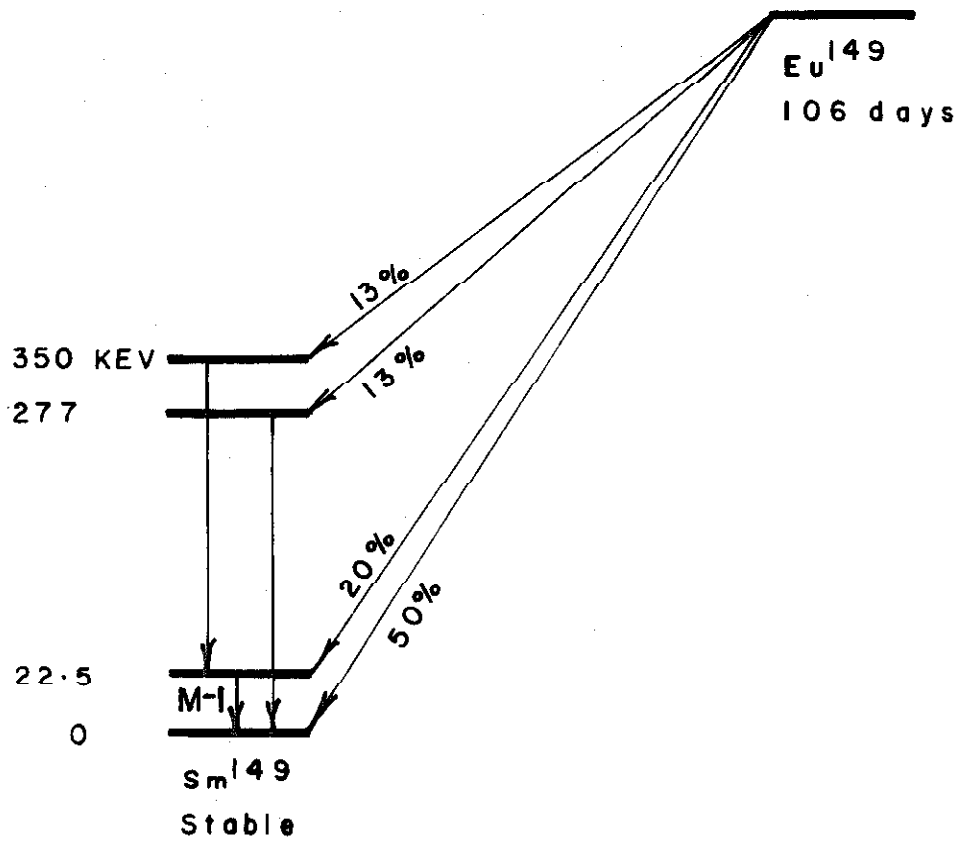

FIGURE 1

Partial Nuclear Level Scheme of Sm^{149}

Additional Information:

Sm^{149} natural isotopic abundance 13.8%.

Nuclear parameters:

Ground state:

$I = 7/2$

$\mu = .648 \pm .012\ \mu_N$ (32)

$Q = .060 \pm .001$ (61)

Excited state (22 keV):

$I = 5/2$ (43)

$\mu_{ex}/\mu_{gr} = 1.26 \pm .04$ (43)

$T_{1/2} = 7.6 \pm .5 \times 10^{-9}$ sec (42)

bations on the ion from its environment to two: one specifying the strength of the exchange interactions coupling the samarium ion spins and one specifying the strength of the crystalline electric field arising from the charges of the surrounding ions. From these Laves phase alloys we chose $SmAl_2$, as the high reported Curie temperature of 122 ^{o}K[5] is of experimental convenience, and the compound is easy to prepare. Moreover, this compound has the unique feature that the samarium ion may be expected to experience crystalline electric field interactions of comparable size in a metallic environment, both interactions being substantially affected by multiplet admixtures.

II. THEORY OF THE MAGNETIC PROPERTIES OF $SmAl_2$

A. Properties of the Free Trivalent Samarium Ion

Fundamental to the understanding of the trivalent samarium ion is the fact that in samarium, as in all the rare earths, the 4f electrons are deeply buried in the ion core and are shielded from external influences by filled 5s and 5p sub-shells. Because of this shielding of the 4f electrons, the spin orbit coupling is stronger than all external perturbations[6], and the free ion states $|J, M\rangle$ offer a suitable basis for the diagonalization of external perturbations on the ion. In samarium first order perturbation theory is likely to be inadequate because of the proximity of the $J = 7/2$ multiplet to the $J = 5/2$ ionic ground state (Figure II). For a physical understanding of the results of perturbation theory it is convenient to note that in samarium the spin and orbital angular momentum are oppositely directed in the low lying multiplets. The free ion g-factor therefore is small in the ground multiplet, $g = 2/7$.

B. Interactions in $SmAl_2$ in the Ferromagnetic State

The two major perturbations acting on the samarium ion in materials capable of magnetic ordering are the crystalline electric field and the exchange interaction between ionic spins.

1. The crystalline electric field (CEF)

The CEF perturbation arises from the interaction of the electrons of the partially filled 4f shell of the rare earth ion with the electric field produced by the charges of the surrounding ions. In

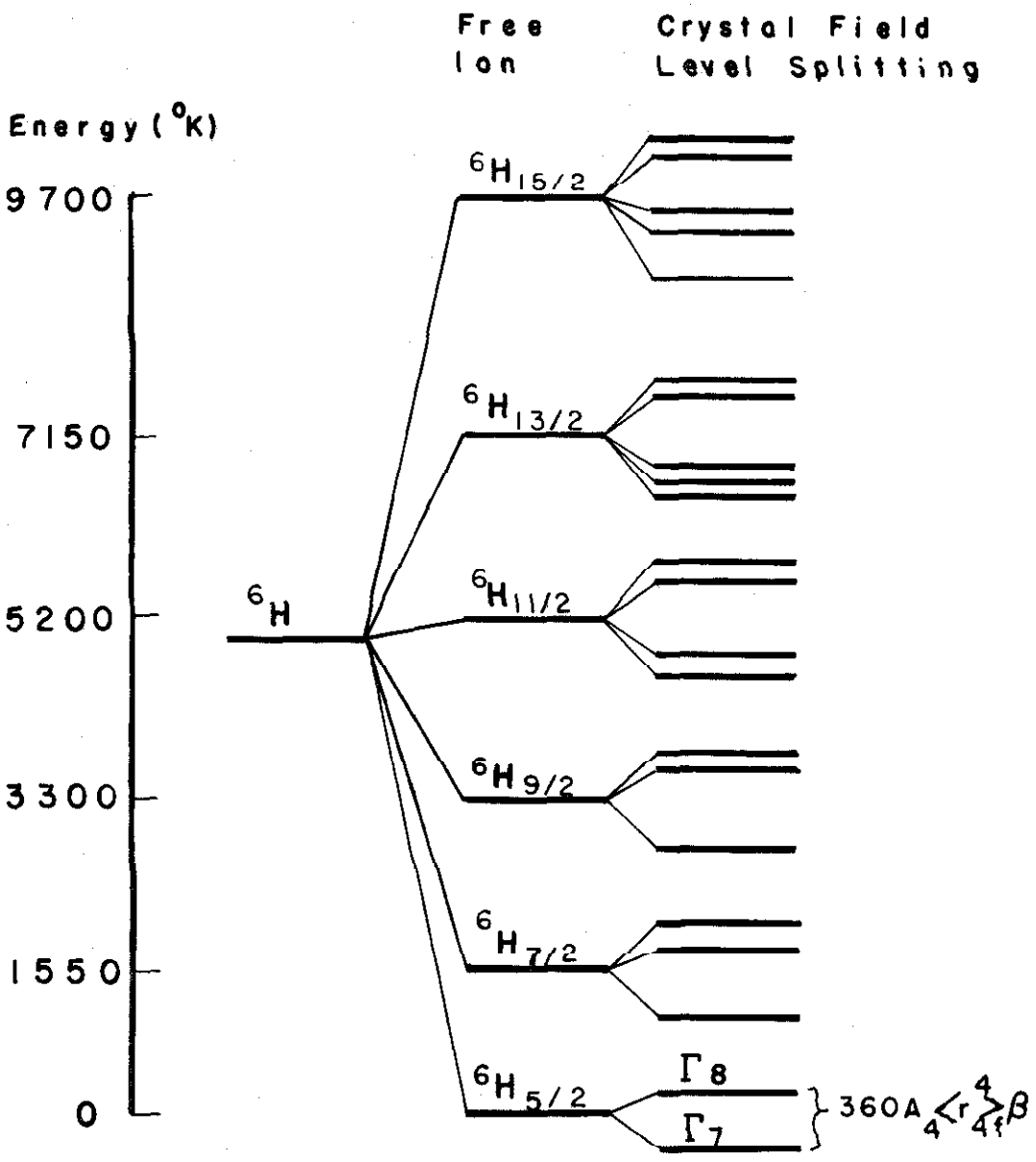

FIGURE II

Structure of the Ground Term of Sm^{3+} (Splitting by the Crystal Field is Shown Schematically---Splitting of the Ground Multiplet is Exaggerated by a Factor of About Five)

$SmAl_2$ the sites of the samarium ions are equivalent. Each is surrounded by 12 aluminum ions as its nearest neighbors, and four samarium ions as its next nearest neighbors in tetrahedral symmetry (Figure III)[7]. The three-fold axis of the tetrahedron coincides with the body diagonal of the cubic unit cell.

The potential energy describing the interaction between the CEF and a negative charge at position (r, θ, φ) within the ion centered at the origin may be represented by the following expansion:

$$-eV(r, \theta, \varphi) = \sum_{n} \sum_{m=-n}^{+n} \sqrt{4\pi/2n+1}\ A_n^m r^n Y_n^m(\theta, \varphi) \quad , \tag{1}$$

if one assumes that there is no overlap between the charge distributions on different ions[8]. The parameters A_n^m are determined by the charge distribution surrounding the central ion and the $Y_n^m(\theta, \varphi)$ are spherical harmonics. In the rare earth series selection rules on the single particle 4f electron matrix elements of this potential allow one to neglect all terms of the series but those for $n = 2, 4, 6$[9]. For the tetrahedral samarium site in $SmAl_2$ the terms with $n = 2$ do not appear, and relations between the A_n^m can be derived to give* [10]

$$\begin{aligned} -eV(r, \theta, \varphi) = {} & A_4 r^4 \sqrt{4\pi/9}\ \left\{Y_4^0 + \tfrac{1}{2}\sqrt{10/7}\,(Y_4^4 + Y_4^{-4})\right\} \\ & + A_6 r^6 \sqrt{4\pi/13}\ \left\{Y_6^0 - \tfrac{1}{2}\sqrt{14}\,(Y_6^4 + Y_6^{-4})\right\} . \end{aligned} \tag{2}$$

---

* Note that the A_4 and A_6 of the present work have been so normalized that $A_4\langle r^4\rangle_{4f}\beta$ is equal to the B_4 of Lea et al.[14], and similarly for A_6. The D_4 and D_6 of Low are normalized differently.

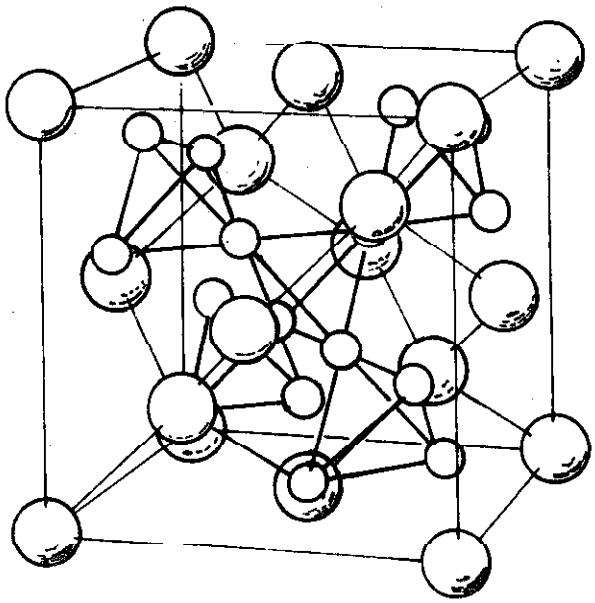

FIGURE III

THE UNIT CELL OF $SmAl_2$

= Samarium

= Aluminum

Although the site symmetry is tetrahedral, the resulting potential function is cubic with the same axes of symmetry as the cubic unit cell[11]. The increase in symmetry results from the stringent selection rules on the matrix elements. The effect of this perturbation in all orders of perturbation theory is to separate the ground multiplet into a doublet and a quartet (Γ_7 and Γ_8, respectively, when the eigenstates are classified under the representations of the cubic group)[12]. The energies and eigenfunctions resulting from this potential may be computed, in first order perturbation theory, using the well-known technique of equivalent operators[13]. The sixth order potential does not enter in this approximation, again because of angular momentum selection rules on the $J = 5/2$ ground state, and the energy separation between the two CEF levels becomes $\Delta E = 360\, A_4 \langle r^4 \rangle_{4f} \beta$ where β is a reduced matrix element of the CEF in the ground state and $\langle r^4 \rangle_{4f}$ is the expectation value of r^4 for a single 4f electron. If A_4 is positive, the doublet lies lowest[14]. The CEF eigenfunctions are given in Table I.

The presence of a CEF interaction comparable to room temperature in the rare earth salts has long been known and has been extensively studied, most effectively by means of optical spectroscopy. Although one might expect that, because of the strong shielding effects of the conduction electrons, the CEF would be small in the rare earth metals and alloys, it is thought that crystalline electric fields of significant size exist in these substances also. Their existence is invoked to explain the diverse spin configurations observed in the magnetically ordered pure rare earth metals[15, 16]. In praesodymium metal Bleaney requires a CEF interaction of the order of 200 ^{o}K to fit the low temperature specific heat data, and estimates on the basis of specific heat and susceptibility measure-

	z = (1, 0, 0)	z = (1, 1, 1)
Γ_7	$\left\|\frac{5}{2}\alpha\right\rangle = \frac{1}{\sqrt{6}}\left\|\frac{5}{2}\,\frac{5}{2}\right\rangle - \sqrt{\frac{5}{6}}\left\|\frac{5}{2}\,-\frac{3}{2}\right\rangle$	$\left\|\frac{5}{2}\alpha\right\rangle = \frac{2}{3}\left\|\frac{5}{2}\,\frac{5}{2}\right\rangle - \frac{\sqrt{5}}{3}\left\|\frac{5}{2}\,-\frac{1}{2}\right\rangle$
	$\left\|\frac{5}{2}\beta\right\rangle = \frac{1}{\sqrt{6}}\left\|\frac{5}{2}\,-\frac{5}{2}\right\rangle - \sqrt{\frac{5}{6}}\left\|\frac{5}{2}\,\frac{3}{2}\right\rangle$	$\left\|\frac{5}{2}\beta\right\rangle = \frac{2}{3}\left\|\frac{5}{2}\,-\frac{5}{2}\right\rangle + \frac{\sqrt{5}}{3}\left\|\frac{5}{2}\,\frac{1}{2}\right\rangle$
Γ_8	$\left\|\frac{5}{2}\varkappa\right\rangle = -\sqrt{\frac{5}{6}}\left\|\frac{5}{2}\,-\frac{5}{2}\right\rangle - \frac{1}{\sqrt{6}}\left\|\frac{5}{2}+\frac{3}{2}\right\rangle$	$\left\|\frac{5}{2}\varkappa\right\rangle = \frac{\sqrt{5}}{3}\left\|\frac{5}{2}\,-\frac{5}{2}\right\rangle - \frac{2}{3}\left\|\frac{5}{2}\,\frac{1}{2}\right\rangle$
	$\left\|\frac{5}{2}\Lambda\right\rangle = \left\|\frac{5}{2}\,\frac{1}{2}\right\rangle$	$\left\|\frac{5}{2}\lambda\right\rangle = \left\|\frac{5}{2}\,\frac{3}{2}\right\rangle$
	$\left\|\frac{5}{2}\mu\right\rangle = -\left\|\frac{5}{2}\,-\frac{1}{2}\right\rangle$	$\left\|\frac{5}{2}\mu\right\rangle = \left\|\frac{5}{2}\,-\frac{3}{2}\right\rangle$
	$\left\|\frac{5}{2}\nu\right\rangle = \sqrt{\frac{5}{6}}\left\|\frac{5}{2}\,\frac{5}{2}\right\rangle + \frac{1}{\sqrt{6}}\left\|\frac{5}{2}\,-\frac{3}{2}\right\rangle$	$\left\|\frac{5}{2}\nu\right\rangle = \frac{\sqrt{5}}{3}\left\|\frac{5}{2}\,\frac{5}{2}\right\rangle + \frac{2}{3}\left\|\frac{5}{2}\,-\frac{1}{2}\right\rangle$

Table I

Crystal field eigenfunctions for J = 5/2

The eigenfunctions are expanded in terms of eigenfunctions $|J, M\rangle$ of J_z for the two cases that the four-fold axis (1, 0, 0) or the three-fold axis (1, 1, 1) is chosen as the z-axis.

ments that crystal fields of comparable size exist in cerium and neodymium[17,18] In other papers[11,19] he attributes to a crystal field interaction of this order of magnitude the reduction of the saturation magnetization in certain Laves phases to a value less than that expected from the free ion magnetic moment of the rare earth constituent. Low temperature measurements by White et al. (20) of the susceptibility of the paramagnetic Laves phase $CeAl_2$ require a CEF interaction of 200 ^{o}K to fit the data. It thus seems not unreasonable to expect a crystal field interaction of this same order of magnitude in $SmAl_2$.

2. The Exchange Interaction

The current understanding of the magnetic properties of the rare earth metals and alloys in the ordered state is that the 4f electron orbitals on different ions do not significantly overlap, and the 4f electrons are not delocalized into a conduction band[21]. This has two important consequences. First, it is a good approximation, in contrast to the iron group metals, to view the magnetism of the rare earth metals as arising from the localized moments of the 4f electrons at the sites of the rare earth ions. Second, direct exchange between different rare earth sites through the overlap of 4f orbitals is unlikely to contribute significantly to the magnetic ordering. Some form of indirect exchange is required.

Such an indirect coupling between ion spins is provided by the conduction electrons in the Ruderman-Kittel-Kasuya-Yosida (RKKY) mechanism[22,23,24]. With this mechanism, an exchange interaction between a conduction electron spin and ion core spin at one site aligns the spin of that conduction electron until it suffers

another exchange interaction with an ion spin at a second site. When these interactions are summed over all conduction electrons, it is found that there is an effective interaction between all the sites of the form

$$-2 \sum_{i>j} \mathcal{J}(r_{ij})\, \vec{S}_i \cdot \vec{S}_j \quad ,$$

where $\mathcal{J}(r_{ij})$ is a slowly decreasing oscillatory function of the distance r_{ij} between sites i and j, and $\vec{S}_i$ and $\vec{S}_j$ are the spins at those sites.

To derive the magnetic ordering properties of the material from this interaction without approximation is an unsolved theoretical problem, and we shall make use of the molecular field approximation* (25). The effect of all the other spins in the sample acting on a spin $\vec{S}$ is approximated by a fictitious magnetic field $\vec{H}_S$ acting on $\vec{S}$, giving an interaction at the site of the samarium ion of the form

$$-\vec{H}_S \cdot \vec{S}\mu_B = -H_S S_Z \mu_B \quad , \tag{3}$$

where H_S is presumed to define the axis of quantization z. The exchange field is taken to be proportional to the thermal average of S_z over the eigenstates $|i\rangle$ of the ion whose energies E_i and spins $S_{z,i}$ are themselves functions of H_S.

$$H_S = \Lambda\mu_B \langle S_z \rangle_T = \Lambda\mu_B \sum_i S_{z,1} \exp(-E_1/kT)/Z$$
$$Z = \sum_i \exp(-E_i/kT) \quad , \tag{4}$$

---

* The use of the molecular field theory to relate the saturation magnetization at 0 ^{o}K and the Curie temperature to the crystal field has been discussed by Bleaney [25].

where $S_{z,i} = \langle i | S_z | i \rangle$.

The constant of proportionality Λ may be determined from the condition that the exchange field should vanish at the Curie point T_c. Near this temperature the energies and spins of the eigenstates $|i\rangle$ may be expanded in powers of H_s. Keeping only terms up to first order in H_s, and using Equation (4), we have

$$1/\Lambda = \sum_i (\mu_B^2 S_{z,i}(0)^2/kT_c + \mu_B \frac{\partial S_{z,i}}{\partial H_s}\Big|_{H_s = 0}) \exp(-E_i(0)/kT_c)/Z(0) \tag{5}$$

$$Z(0) = \sum_i \exp(-E_i(0)/kT_c) \ .$$

Once Λ is determined, the exchange field and mean spin $\langle S_z \rangle_T$ are determined implicitly by Equation (4) which may be solved by an iterative procedure.

3. Diagonalization of the Combined Interaction

Taking into account the two perturbations we have discussed above, the Hamiltonian for a trivalent samarium ion in a substance capable of magnetic ordering becomes

$$H = H_0 + H_{cef} - H_s \mu_B S_z \ , \tag{6}$$

where H_0 is the unperturbed free ion Hamiltonian and the last two terms are the perturbations due to the CEF and exchange, respectively. In $SmAl_2$ the reported Curie point is 122 ^oK[5] which is comparable in size to our estimate of the CEF, and it therefore seems not to be a good approximation to treat one of the two perturbations

separately from the other. The magnetic anisotropy energy must have the symmetry of the cubic CEF potential (Equation 2) and is most likely to have a minimum in the direction of one of the high symmetry axes of the cubic cell: either a four-fold axis, the cube edge, or a three-fold axis, the body diagonal of the cube. We therefore shall only consider the case in which the axis of spontaneous magnetization lies parallel to one of these high symmetry axes. Because the two perturbation energies in $SmAl_2$ are a significant fraction of the 1500 ^{o}K which separate the J = 5/2 and J = 7/2 multiplets of the ion, we expect that mixing of these multiplets plays an important role. We shall first discuss the diagonalization of the Hamiltonian in the case where this state mixing is neglected and later take it into account.

a. Admixture of next higher multiplet neglected: first order perturbation theory

Upon beginning the diagonalization of the perturbation matrix in the ground multiplet of the ion, it is convenient to introduce certain dimensionless parameters. The energy separation between the two CEF states in the limit of vanishing exchange is taken to be 3Δ where $\Delta = 120\ A_4 \langle r^4 \rangle_{4f}\ \beta$ as long as multiplet mixing is neglected and is positive in the case that Γ_7 lies lowest. We then diagonalize the dimensionless Hamiltonian $H' = H/\Delta$ giving dimensionless energies $\epsilon_i = E_i/\Delta$. Introducing $H'_{cef} = H_{cef}/\Delta$ and a parameter y giving the relative strength of the CEF and exchange

$$y = (g - 1)\,\mu_B H_s/\Delta \ , \qquad (7)$$

we have

$$H' = H'_{cef} - y J_z \quad . \tag{8}$$

It is convenient to choose the CEF eigenfunctions listed in Table I as a basis for the diagonalization of this operator. In this case the matrix breaks down into two by two submatrices and the diagonalization is easily carried out. The matrix of H' is given in Table II for the two cases that the spontaneous magnetization lies along a four-fold or three-fold axis of the cubic unit cell. The eigenvalues ϵ_i are given in Table III as a function of the relative strength y of the exchange and CEF. The results of this diagonalization are depicted in Figures IV and V. In Figure IV the transition from the case of a pure crystal field, where the eigenfunctions are those of Table I, to the case of a pure exchange field, where J_z is diagonal, is shown in its entirety[26]. The ratio of the energy of each state to the strength of the combined interaction (CEF + exchange) is plotted against the ratio of the strength of the exchange to that of the combined interaction. In Figure V the scales are chosen so that the expectation value of J_z in each state can be estimated; the ratio of the energy of each state to the strength of the CEF is plotted against the ratio y of the exchange to the CEF. The expectation value of J_z in each state is given by the negative of the slope of corresponding energy plotted as a function of y.

b. Admixture of next higher multiplet included: second order perturbation theory

In second order perturbation theory the energies of the states arising from the ground multiplet are given by[27]

$$\langle J,i \,|\, H_{cef} - \mu_B S_z H_x - \sum_{J'}{}' (H_{cef} - \mu_B S_z H_x) \frac{P_{J'}}{E_J} (H_{cef} - \mu_B S_z H_x) \,|\, J,i \rangle \,, \tag{9}$$

z = four-fold axis

	α	ν	β	$\varkappa$	Λ	μ
α	$-2+\frac{5}{6}y$	$-2\frac{\sqrt{5}}{3}y$				
ν	$-2\frac{\sqrt{5}}{3}y$	$1-\frac{11}{6}y$				
β			$-2-\frac{5}{6}y$	$-\frac{2}{3}\sqrt{5}y$		
$\varkappa$			$-\frac{2}{3}\sqrt{5}y$	$1+\frac{11}{6}y$		
Λ					$1-\frac{1}{2}y$	0
μ					0	$1+\frac{1}{2}y$

z = three-fold axis

	α	ν	β	$\varkappa$	Λ	μ
α	$-2+\frac{5}{6}y$	$\frac{2}{3}\sqrt{5}y$				
ν	$\frac{2}{3}\sqrt{5}y$	$1+\frac{7}{6}y$				
β			$-2-\frac{5}{6}y$	$-\frac{2}{3}\sqrt{5}y$		
$\varkappa$			$-\frac{2}{3}\sqrt{5}y$	$1-\frac{7}{6}y$		
Λ					$1-\frac{3}{2}y$	0
μ					0	$1+\frac{3}{2}y$

Table II

Reduced Hamiltonian Matrix H'

$H' = H/\Delta = H_{cef}/\Delta - y J_z$

(CEF eigenfunctions of Table I as basis)

Magnetization along (1, 0, 0)	Magnetization along (1, 1, 1)
$\epsilon_{\alpha'} = -1/2 - 1/2y - 1/2\sqrt{9 - 16y + 16y^2}$	$\epsilon_{\alpha'} = -1/2 + y - 1/2\sqrt{9 + 2y + 9y^2}$
$\epsilon_{\beta'} = -1/2 + 1/2y - 1/2\sqrt{9 + 16y + 16y^2}$	$\epsilon_{\beta'} = -1/2 - y - 1/2\sqrt{9 - 2y + 9y^2}$
$\epsilon_{\kappa'} = -1/2 + 1/2y + 1/2\sqrt{9 + 16y + 16y^2}$	$\epsilon_{\kappa'} = -1/2 - y + 1/2\sqrt{9 - 2y + 9y^2}$
$\epsilon_{\Lambda'} = 1 - 1/2y$	$\epsilon_{\Lambda'} = 1 - 3/2y$
$\epsilon_{\mu'} = 1 + 1/2y$	$\epsilon_{\mu'} = 1 + 3/2y$
$\epsilon_{\nu'} = -1/2 - 1/2y + 1/2\sqrt{9 - 16y + 16y^2}$	$\epsilon_{\nu'} = -1/2 + y + 1/2\sqrt{9 + 2y + 9y^2}$

Table III

Eigenvalues of the Reduced Hamiltonian H' of Table II, $\epsilon_i = E_i/\Delta$

z-axis = (1, 0, 0)	z-axis = (1, 1, 1)
$J_{z\alpha'} = 1/2 + \frac{8y - 4}{\sqrt{9 - 16y + 16y^2}}$	$J_{z\alpha'} = -1 + 1/2\ \frac{9y + 1}{\sqrt{9 + 2y + 9y^2}}$
$J_{z\beta'} = -1/2 + \frac{8y + 4}{\sqrt{9 + 16y + 16y^2}}$	$J_{z\beta'} = 1 + 1/2\ \frac{9y - 1}{\sqrt{9 - 2y + 9y^2}}$
$J_{z\kappa'} = -1/2 - \frac{8y + 4}{\sqrt{9 + 16y + 16y^2}}$	$J_{z\kappa'} = 1 - 1/2\ \frac{9y - 1}{\sqrt{9 - 2y + 9y^2}}$
$J_{z\Lambda'} = 1/2$	$J_{z\Lambda'} = 3/2$
$J_{z\mu'} = -1/2$	$J_{z\mu'} = -3/2$
$J_{z\nu'} = 1/2 - \frac{8y - 4}{\sqrt{9 - 16y + 16y^2}}$	$J_{z\nu'} = -1 - 1/2\ \frac{9y + 1}{\sqrt{9 + 2y + 9y^2}}$

Table IV

Expectation value of J_z in the eigenstates of $H' = H_{CEF}/\Delta - yJ_z$

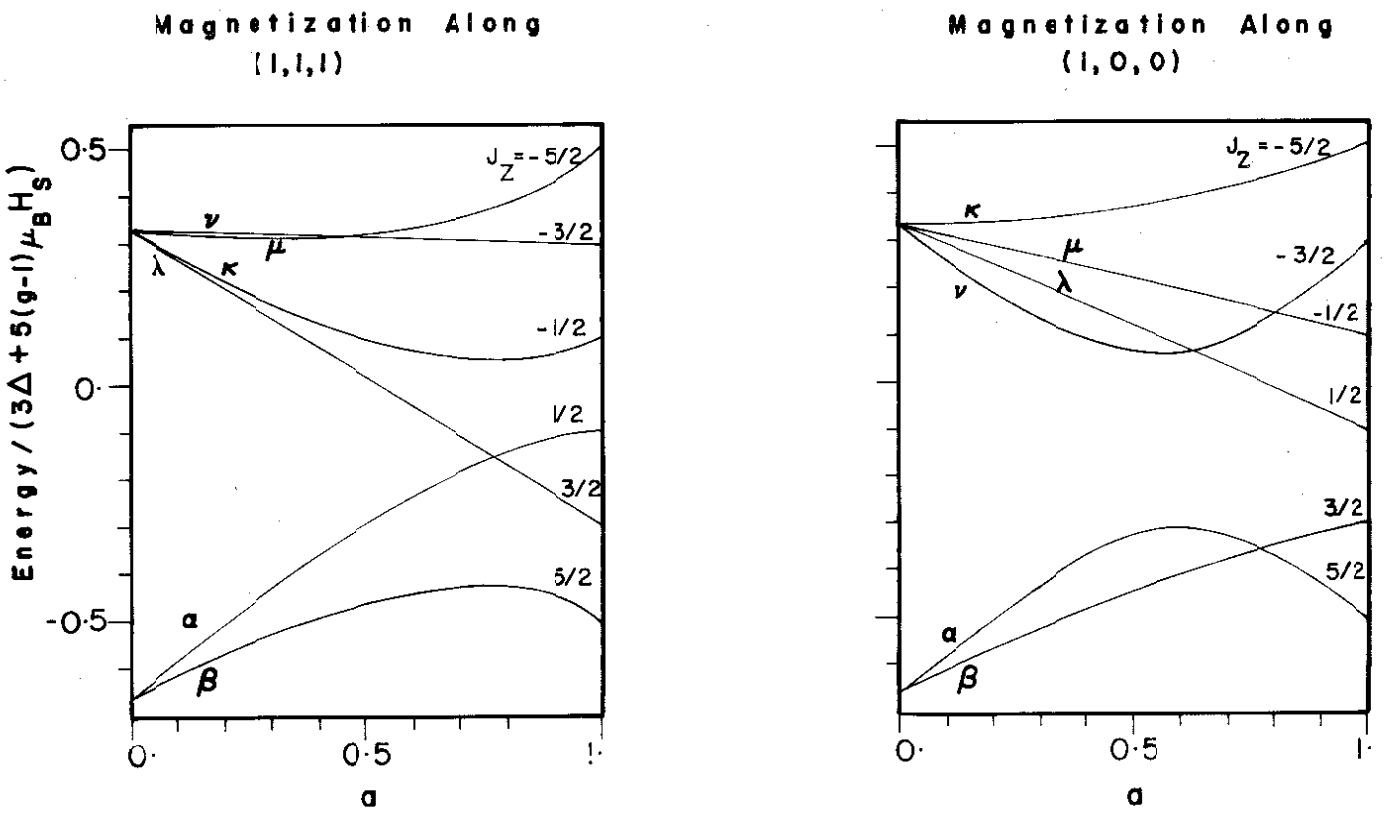

FIGURE IV

The Transition From Pure CEF To Pure Exchange.

The relative energy of each state is plotted against the parameter a of White and Andelin,[26]

$$a = 5(g-1)\mu_B H_S / (3\Delta + 5(g-1)\mu_B H_S)$$

$a = 0$ CEF only

$a = 1$ Exchange only

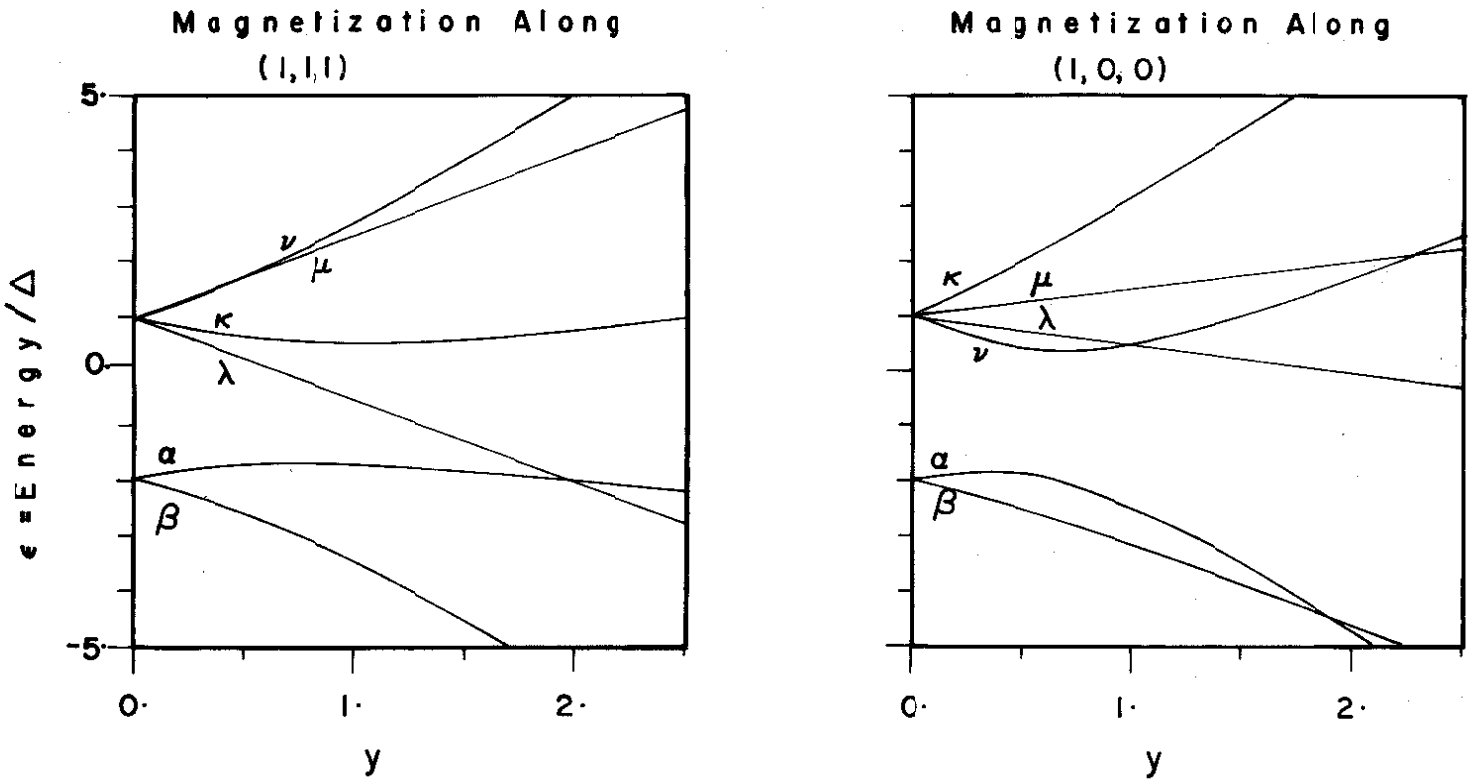

FIGURE V

The eigenvalues ϵ_i of Table III are shown as functions of the parameter y

$$y = (g-1)\mu_B H_S / \Delta$$

$$\langle J_z \rangle_i = -\frac{d\epsilon_i}{dy}$$

where $|J,i\rangle$ are the eigenstates resulting from the application of first order perturbation theory to the ground multiplet $J = 5/2$, E_J, is the unperturbed energy separation between the ground multiplet and the multiplet of total angular momentum J', $P_{J'} = \sum_{M'}' |J', M'\rangle\langle J', M'|$ is the projector for the multiplet J', and the prime on the summation indicates that terms with $J = J'$ are excluded. Three contributions appear in the summation over excited multiplets J'. The first of these is the term second order in the CEF. In the present context this is the least important contribution, for, aside from a downward displacement of the center of gravity of the ground multiplet not observable with the measuring technique used in this study, the sole effect of this part is a renormalization of the energy separation of the Γ_7 doublet and Γ_8 quartet. For the trivalent samarium ion diluted in $LaCl_3$, the overall crystal field splitting of the ground multiplet of the ion is 64 cm^{-1} and, while the inclusion of admixtures of higher lying multiplets by the crystal field leads to a downward displacement of the center of gravity of the multiplet by 12%, the relative displacement of the sublevels of the ground multiplet with respect to each other is on the order of 1%[1]. We expect that this renormalization of the crystal field is small in our case also. Moreover, as these small alterations in the relative energies of the states of the ground multiplet are independent of the exchange field, the iteration procedure to solve the molecular field equations is not much affected, and we have not included this contribution in the calculations.

The remaining two contributions to the second order energies are the contribution second order in the exchange and the interference term between the exchange and crystal field. In the interference term the A_6 part of the CEF may contribute as well as the A_4 part, adding a third parameter to the theory.

Bleaney[11], on the basis of an electrostatic model of the CEF taking into account nearest and next nearest neighbors of the rare earth ion has estimated that the contribution of the A_6 part of the CEF should be of minor importance in the cubic rare earth-nickel intermetallic compounds, isomorphic to $SmAl_2$. White et al.[20] have observed that the apparent CEF needed to account for their susceptibility data may be accounted for on the basis of such a model, assuming trivalent cerium ions and an average compensating charge of -1.5e on the aluminum ions. If we accept this model, the contribution of the A_6 part of the CEF to the second order corrections is at least three times smaller than the A_4 part, and we have followed Bleaney in neglecting A_6.

The contributions to the second order corrections to the energies are listed in Table V, with equivalent operators that aid in their evaluation. These operators are derived from the matrix elements given by Elliott and Stevens[28] and by Judd[29]. The matrix of the equivalent operators $M_{5/2,\,7/2}(J)$ and $V_{5/2,\,7/2}(J)$ are given in Tables VI and VII respectively with the J = 5/2 CEF eigenfunctions of Table I chosen as a basis.

C. The magnetic properties of ferromagnetic $SmAl_2$

The magnetic moment is the sum of the moments due to spin and orbital angular momenta

$$\vec{\mu} = (\vec{L} + 2\vec{S})\mu_B = (\vec{J} + \vec{S})\mu_B \ . \qquad (10)$$

As $\vec{J}$ can have only zero matrix elements between multiplets of different total angular momentum, admixture of an excited multiplet

Expectation value of the energy to second order:

$$E_i = \langle \frac{5}{2}, i | H_{CEF} - \mu_B S_z H_s - \sum_{J'}{}' \frac{(H_{CEF} - \mu_B S_z H_s) P_{J'} (H_{CEF} - \mu_B S_z H_s)}{E_{J'}} | \frac{5}{2}, i \rangle$$

with $P_{J'} = \sum_{M} |J', M\rangle\langle J', M|$

Contributions to the second order corrections:

CEF x CEF

$$- \langle \frac{5}{2}, i | \sum{}' \frac{H_{CEF} P_{J'} H_{CEF}}{E_{J'}} | \frac{5}{2}, i \rangle$$

Exchange x Exchange

$$-\mu_B{}^2 H_s{}^2 \langle \frac{5}{2}, i | \frac{S_z P_{7/2} S_z}{E_{7/2}} | \frac{5}{2}, i \rangle = - \frac{g_1{}^2 \mu_B{}^2 H_s{}^2}{E_{7/2}} \langle \frac{5}{2}, i | M_{5/2,7/2}(\hat{J}) | \frac{5}{2}, i \rangle$$

Exchange x CEF

$$+ \frac{\mu_B H_s}{E_{7/2}} \langle \frac{5}{2}, i | H_{CEF} P_{7/2} S_z + S_z P_{7/2} H_{CEF} | \frac{5}{2}, i \rangle$$

$$= 120 \frac{g_1 \mu_B H_s A_4 \langle r^4 \rangle_{4f}}{E_{7/2}} \langle \frac{5}{2}, i | V_{5/2,7/2}(\hat{J}) | \frac{5}{2}, i \rangle$$

Definition of equivalent operators:

$$M_{5/2,7/2}(\hat{J}) = \frac{49}{4} - J_z{}^2$$

$$120\ V_{5/2,7/2}(\hat{J}) = \mathcal{V}_4{}^0(\hat{J}) + 5\,\mathcal{V}_4{}^4(\hat{J}) \qquad \text{for } z = (1,0,0)$$

$$= -\mathcal{V}_4{}^0(\hat{J}) + 20/2\,\mathcal{V}_4{}^3(\hat{J}) \qquad \text{for } z = (1,1,1)$$

$$\mathcal{V}_4{}^0(\hat{J}) = 2(\frac{40}{4} - J_z{}^2) J_z (7J_z{}^2 - \frac{127}{4})$$

$$\mathcal{V}_4{}^4(\hat{J}) = \frac{1}{10} [J_z(J_+{}^4 + J_-{}^4) + (J_+{}^4 + J_-{}^4) J_z]$$

$$\mathcal{V}_4{}^3(\hat{J}) = \frac{1}{40} [4J_z{}^2(J_+{}^3 + J_-{}^3) + 4(J_+{}^3 + J_-{}^3)J_z{}^2 - 53(J_+{}^3 + J_-{}^3)]$$

$$J_\pm = J_x \pm i J_y$$

Table V

Second order corrections to the state energies

Definition	Notation of present work	Notation of Elliott and Stevens	Value
$\langle 5/2 \| \mu \| 5/2 \rangle / \mu_B$	g	$\langle 5/2 \| \Lambda \| 5/2 \rangle$	0.2857
$\langle 5/2 \| \mu \| 7/2 \rangle / \mu_B$	g_1	$\langle 5/2 \| \Lambda \| 7/2 \rangle$	0.3912
$\langle 5/2 \| S \| 5/2 \rangle$	$g - 1$	$\langle 5/2 \| \Lambda \| 5/2 \rangle - 1$	-.7143
$\langle 5/2 \| S \| 7/2 \rangle$	g_1	$\langle 5/2 \| \Lambda \| 7/2 \rangle$	0.3912
$\langle 5/2 \| L \| 5/2 \rangle$	$2 - g$	$2 - \langle 5/2 \| \Lambda \| 5/2 \rangle$	1.7143
$\langle 5/2 \| L \| 7/2 \rangle$	$-g_1$	$-\langle 5/2 \| \Lambda \| 7/2 \rangle$	-.3912
$\sqrt{\frac{4\pi}{9}} \langle 5/2 \| Y_4 \| 5/2 \rangle$	β	$\langle 5/2 \| \beta \| 5/2 \rangle$	0.002501
$\sqrt{\frac{4\pi}{9}} \langle 5/2 \| Y_4 \| 7/2 \rangle$	β_1	$\langle 5/2 \| \beta \| 7/2 \rangle$	-.008303
$\frac{1}{2\mu_B \langle r^{-3} \rangle_{4f}} \cdot \langle 5/2 \| H_{int} \| 5/2 \rangle$	N	$\langle 5/2 \| N \| 5/2 \rangle$	1.548
$\frac{1}{2\mu_B \langle r^{-3} \rangle_{4f}} \cdot \langle 5/2 \| H_{int} \| 7/2 \rangle$	N_1	$\langle 5/2 \| N \| 7/2 \rangle$	-.3799

Table Va

Reduced matrix elements for various operators

These reduced matrix elements are those appropriate for use with the operator equivalents of Elliott and Stevens. Note that the matrix element of the internal field defined here does not include the contact interaction.

z-axis = four-fold axis

	α	ν	β	$\varkappa$	Λ	μ
α	28/3	$-\frac{2}{3}\sqrt{5}$				
ν	$-\frac{2}{3}\sqrt{5}$	20/3				
β			28/3	$\frac{2}{3}\sqrt{5}$		
$\varkappa$			$\frac{2}{3}\sqrt{5}$	20/3		
Λ					12	0
μ					0	12

z-axis = three-fold axis

	α	ν	β	$\varkappa$	Λ	μ
α	28/3	$-\frac{4}{3}\sqrt{5}$				
ν	$-\frac{4}{3}\sqrt{5}$	26/3				
β			28/3	$-\frac{4}{3}\sqrt{5}$		
$\varkappa$			$-\frac{4}{3}\sqrt{5}$	26/3		
Λ					10	0
μ					0	10

Table VI

Matrix of the operator $M_{5/2,\,7/2}(\hat{J})$ between the crystal field eigenfunctions of Table I

z-axis = four-fold axis

	α	ν	β	$\varkappa$	Λ	μ
α	4	$-\frac{\sqrt{5}}{10}$				
ν	$-\frac{\sqrt{5}}{10}$	3				
β			-4	$-\frac{\sqrt{5}}{10}$		
$\varkappa$			$-\frac{\sqrt{5}}{10}$	-3		
Λ					-3	0
μ					0	3

z-axis = three-fold axis

	α	ν	β	$\varkappa$	Λ	μ
α	+4	$+\frac{\sqrt{5}}{10}$				
ν	$+\frac{\sqrt{5}}{10}$	0				
β			-4	$-\frac{\sqrt{5}}{10}$		
$\varkappa$			$-\frac{\sqrt{5}}{10}$	0		
Λ					+ 8/3	$-\frac{7}{3}\sqrt{2}$
μ					$-\frac{7}{3}\sqrt{2}$	- 8/3

Table VII

Matrix of the operator $V_{5/2,\,7/2}(\hat{J})$ between the crystal field eigenfunctions of Table I.

within the ground term affects the magnetic moment of a state only through the spin.

The hyperfine magnetic field is given by[30]

$$\vec{H}_{int} = 2\mu_B \sum_i \left[\frac{\vec{\ell}_i}{r_i^3} - \left(\frac{r_i^2 \vec{s}_i - 3(\vec{r}_i \cdot \vec{s}_i)\vec{r}_i}{r_i^5} \right) + \frac{8\pi}{3} \vec{s}_i \, \delta(\vec{r}_i) \right] . \qquad (11)$$

The delta function contribution in this summation over electrons is the Fermi contact term, by which s electrons, which fail to contribute by the other terms, produce a contribution to the internal field. In the rare earth region, save for the S state ions such as Gd^{+++} and Eu^{++}, by far the largest contribution to the internal field is made by the 4f electrons via the first two terms in this operator[31] in contrast to the iron group elements, where the dominant contribution is that from the contact term, arising from exchange polarization of core s electrons by the unpaired spins of the partially filled 3 d shell. In metals the contact interaction with the conduction electrons must also be considered, but it is thought to be small. Little is known in detail about the contact interactions, and we shall postpone detailed discussion of them until the contribution from the first two terms of Equation 11 has been treated.

1. Admixtures into the ground multiplet neglected: first order perturbation theory

In first order all vector operators may be represented as equivalent operators proportional to J [13], and in particular, the spin operator appropriate to Equations (4) and (5) is $S_z = (g - 1)J_z$. Given the Curie temperature the numerical

solution of Equations (4) and (5) may be carried out for various values of the CEF parameter Δ using the energies of Table III and the expectation values of J_z given in Table IV. Once the value of H_s has been found, the thermal average $\langle J_z \rangle_T$ is immediately determined:

$$\langle J_z \rangle_T = H_s/(g - 1)\,\Lambda\mu_B \quad . \tag{12}$$

From the temperature dependence of $\langle J_z \rangle_T$ the temperature dependence of the magnetic moment of the ion and the internal field may be determined. The equivalent operators for magnetic moment and internal field are[13]:

$$\begin{aligned} \hat{\mu} &= g\hat{J}_z\,\mu_B \\ \hat{H}_{int} &= 2\mu_B\, N \langle r^{-3} \rangle_{4f}\, \hat{J}_z \quad , \end{aligned} \tag{13}$$

where the Fermi contact interaction has been neglected, $\langle r^{-3} \rangle_{4f}$ is the expectation value of r^{-3} for a 4f electron, and N is a reduced matrix element for the internal field operator (Table V a). The thermally averaged internal field and magnetic moment are then each proportional to the thermal average of J_z, and the ratio is a temperature independent constant:

$$\frac{\langle H_{int} \rangle_T}{\langle \mu \rangle_T} = 2N \langle r^{-3} \rangle_{4f}/g \quad . \tag{14}$$

From Table V a, N = 1.55, and if the value of Bleaney[32], $\langle r^{-3} \rangle_{4f} = 6.72$ atomic units, is used the ratio of the internal field at the nucleus to the magnetic moment of the ion is 4.54×10^6 Oe per Bohr magneton, giving a magnetic field at the nucleus of

3.25×10^6 Oe when the free ion magnetic moment of 0.71 μ_B is attained.

This iterative procedure has been carried out by means of an electronic computer assuming a Curie temperature of 122 ^{o}K. Representative temperature dependences of the magnetic moment and internal field resulting from the calculation are presented in Figure VI. In Figure VII the magnetization and internal field at constant temperature are presented as a function of the CEF splitting. Two important facts emerge from this treatment (cf. Figure VII):

1) For temperatures far enough below the Curie point the spontaneous magnetization computed, assuming the (1, 0, 0) axis to be the axis of magnetization, may differ by an appreciable fraction from that computed if the three-fold (1, 1, 1) is assumed to be the axis of spontaneous magnetization. It will be difficult to saturate polycrystalline samples at low temperatures, and the very low saturation magnetic moment of the samarium ion in $SmAl_2$ at 0 ^{o}K (on the order .2 μ_B) observed by Williams et al.[5] in bulk magnetization measurements using polycrystalline samples may be a result of failure to magnetically saturate the sample. Thus far there have been reported no magnetization measurements using single crystals of $SmAl_2$.

2) The second fact of importance is the decrease of the magnetization and internal field below free ion values as the CEF is increased in magnitude; that is, there is a partial quenching of the total orbital angular momentum by the crystal field. This mechanism has been invoked by Bleaney[11] to account qualitatively for the small values of the saturation magnetization observed by Skrabek and Wallace[33] in the cubic rare earth-nickel intermetallic compounds isomorphic to $SmAl_2$. However, from Figure VII it is

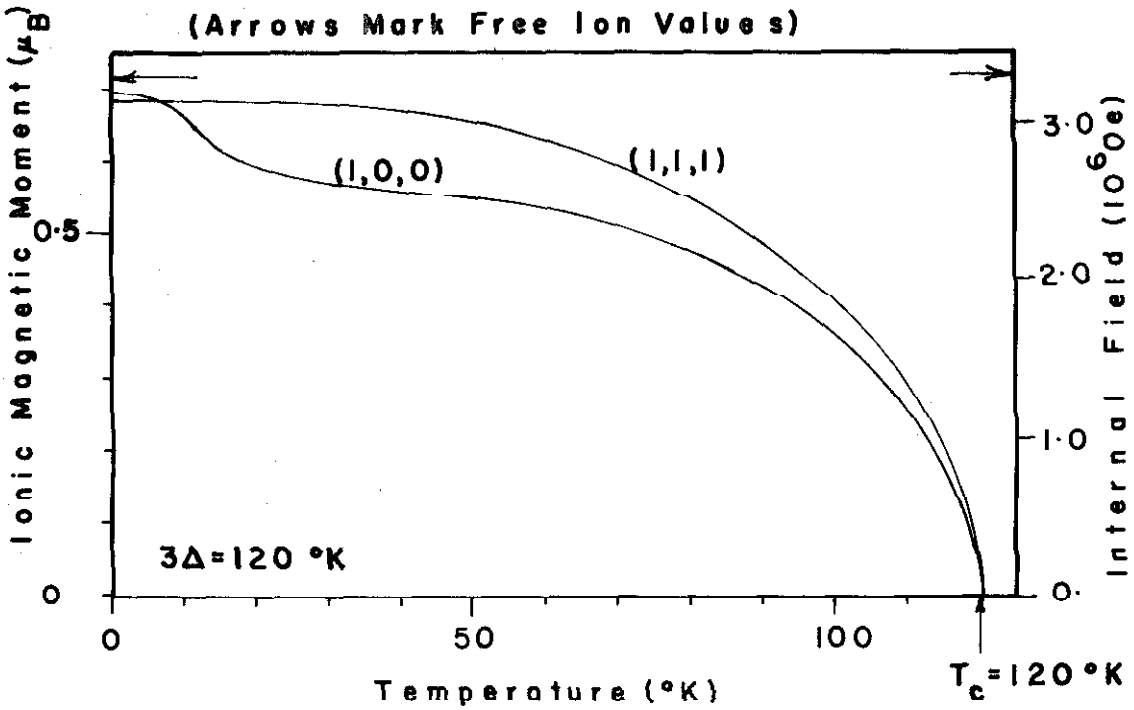

FIGURE VI

Sm^{3+} Magnetic Moment and Internal Field in $SmAl_2$ as a Function of Temperature Neglecting Admixtures of Higher Multiplets, for a CEF Splitting of 120 °K, Exchange Field is Assumed to Lie along (1,1,1) or (1,0,0).

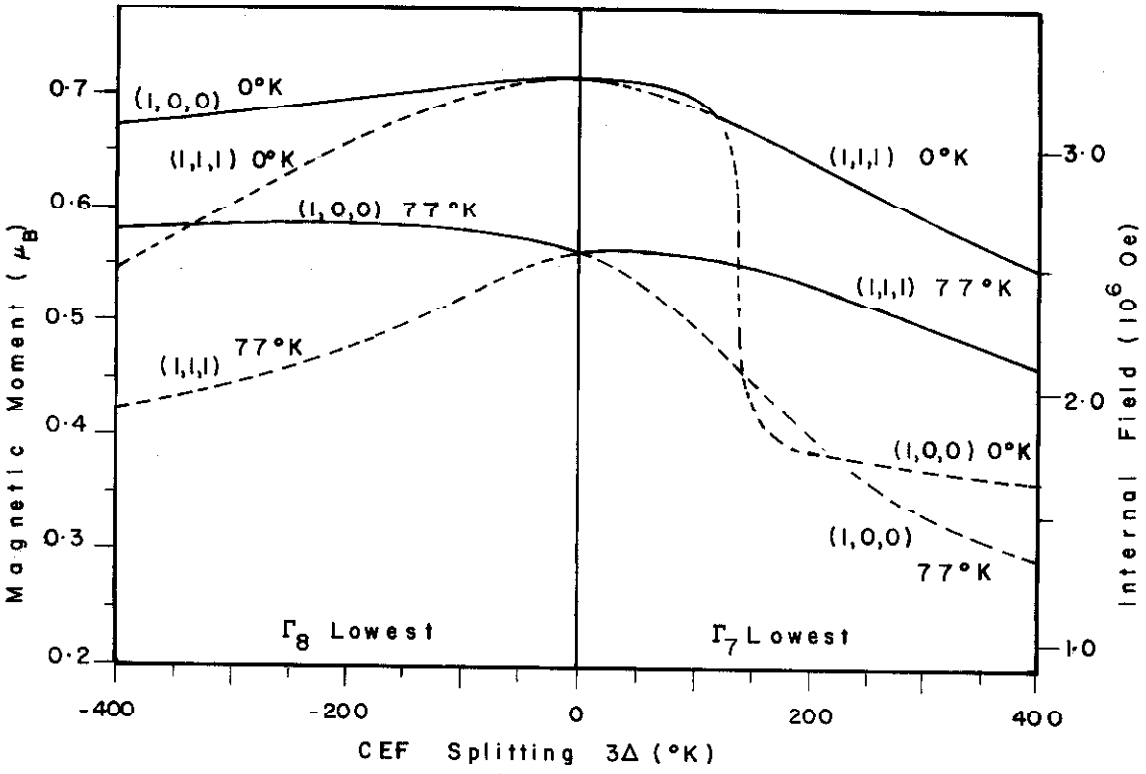

FIGURE VII. Magnetic Moment and Internal Field at $0^{\circ}K$ and $77^{\circ}K$ as a Function of CEF Level Splitting 3Δ with Admixtures of Higher Multiplets Neglected. - In this approximation μ and H_{int} are proportional to each other. The solid curves give the values of the internal field and magnetic moment for the situation in which the energy is a minimum (easy axis of magnetization).

clear that such quenching is not very effective in $SmAl_2$. A crystal field splitting of the ground multiplet of 400 ^{o}K, five times that observed in $SmCl_3$[34] or samarium ethylsulfate[35], is sufficient to give a maximum of a 20% decrease in the saturation magnetization for an easy axis, and the internal field predicted for a spontaneously magnetized sample is decreased by a correspondingly small amount. It remains to see how this picture is altered by the inclusion of the admixture of the next higher multiplet.

2. Admixture of next higher multiplet: second order perturbation theory

In second order perturbation theory the expectation value of an operator $\hat{0}$ in a state $|5/2, i\rangle$ of the ground multiplet is given by[36]

$$\langle \hat{0} \rangle = \langle 5/2, i | \hat{0} - \sum_{J'}{}' \frac{\hat{V} P_{J'} \hat{0} + \hat{0} P_{J'} \hat{V}}{E_{J'}} | 5/2, i \rangle \qquad (17)$$

$$\hat{V} = \hat{H}_{cef} - \mu_B \vec{H}_s \cdot \vec{S} \ .$$

If $\hat{0}$ is a vector operator, the only contribution to the sum over the ionic excited states which need be considered is that from the next higher state $^6H_{7/2}$. The corrections to the magnetic moment, internal field, and spin expectation values are given in Table VIII in terms of the operators and reduced matrix elements introduced in Table V. In particular, N and N_1 are the reduced matrix elements of the internal field operator (excluding the contact term).

The numerical solution of the molecular field Equations (4) and (5) has been carried out as described earlier

$$\langle \hat{O}_z \rangle = \theta_0 \langle \tfrac{5}{2} i | \hat{J}_z | \tfrac{5}{2} i \rangle - \theta_1 \left\{ \langle \tfrac{5}{2} i | \frac{\beta_1}{\beta} \frac{\Delta}{E_{\frac{7}{2}}} \hat{V}_{\frac{5}{2}\frac{7}{2}}(\hat{J}) - \frac{2g_1 \mu_B H_s}{E_{\frac{7}{2}}} \hat{M}_{\frac{5}{2}\frac{7}{2}}(\hat{J}) | \tfrac{5}{2} i \rangle \right\}$$

with $\hat{O}$ a vector operator

$\Delta = 120\, A_4 \langle r^4 \rangle_{4f} \beta$

θ_0, θ_1 reduced matrix elements of $\hat{O}$

For $\hat{O} =$		
$\hat{\mu}$	$\theta_0 = g$	$\theta_1 = g_1$
$\hat{H}_{int}$	$2\mu_B \langle r^{-3} \rangle_{4f} N$	$2\mu_B \langle r^{-3} \rangle_{4f} N_1$
$\hat{S}$	$g - 1$	g_1
$\hat{L}$	$2 - g$	$-g_1$

Table VIII

Second Order Corrections
to Vector Operators

See Table V and Va for definitions of $V_{\frac{5}{2},\frac{7}{2}}(\hat{J})$ and $M_{\frac{5}{2},\frac{7}{2}}(\hat{J})$, and values of reduced matrix elements.

but now including these second order corrections. The spontaneous magnetization, internal field, and exchange field no longer show the same temperature dependence. At any temperature, after the value of the exchange field is determined, the magnetic moment of the ion, and the internal field, must be determined by separate Boltzmann averages over the eigenstates of the ion. In Figure VIII typical results for the magnetic moment and internal field are shown. The results derived from first order perturbation theory for the same crystal field interaction are shown as dashed curves on the graphs for comparison. In Figure IX the magnetic moment and internal field resulting from second order perturbation theory are plotted as a function of the strength of the crystal field interaction.

Comparison of the numerical results of first and second order perturbation theory indicates that the effect of the admixture of the ionic excited multiplet into the ground state is a decrease in the magnetic moment of the ion and an increase in the internal magnetic field at the nucleus from the values given by first order perturbation theory. The difference between the temperature dependence of the ionic magnetic moment and the internal magnetic field are perhaps most are most strikingly indicated in Figure IX. Here it is seen that the magnetization at 0 ^{o}K and 77 ^{o}K are both negligibly small at an overall crystal field splitting of 350 ^{o}K, and this in spite of the fact that the internal magnetic field at the nucleus continues to be of finite size.

D. Summary of Results of Theory

The magnetic properties of $SmAl_2$ depend strongly on the exchange and crystalline electric field acting on the samarium ion,

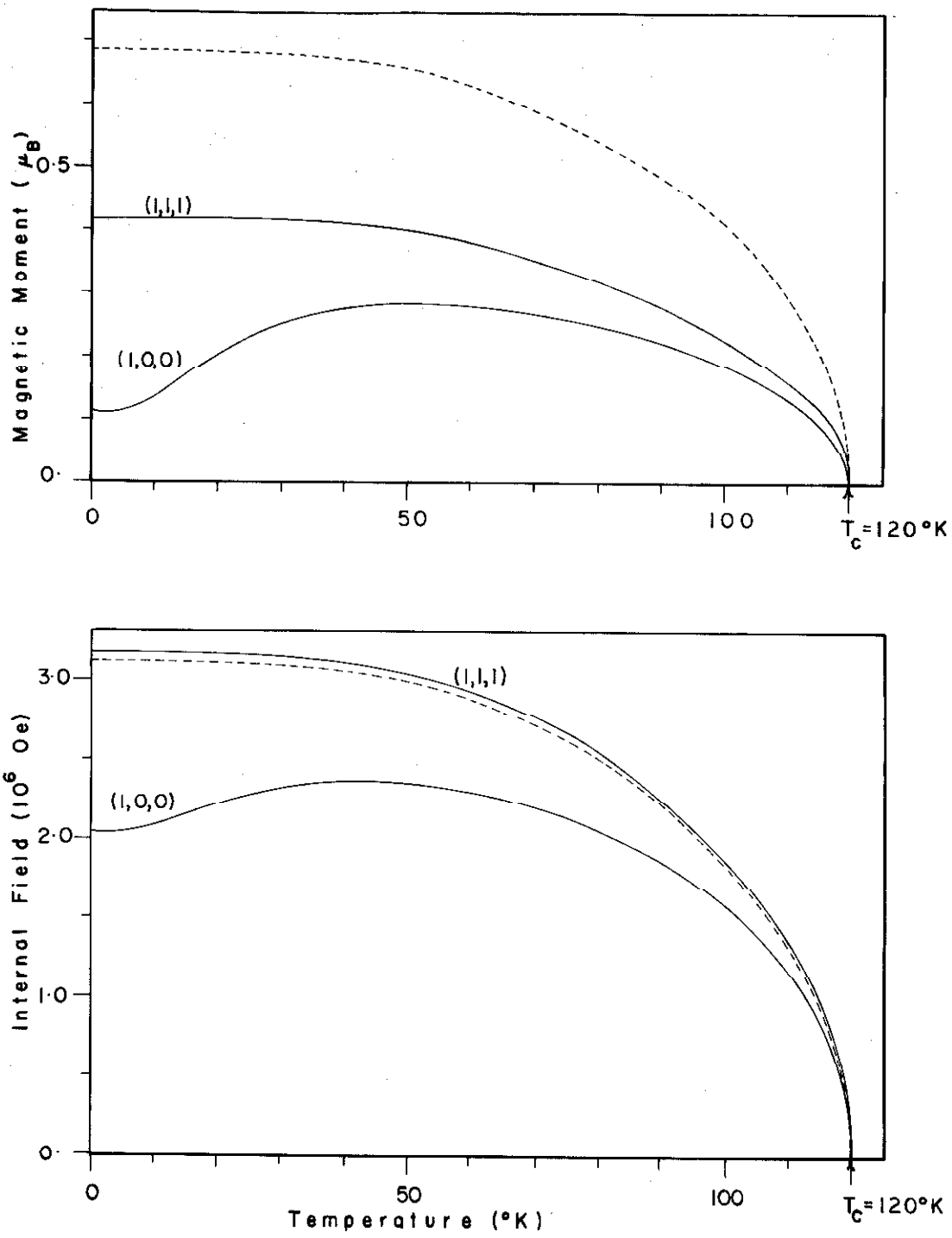

FIGURE VIII Sm^{3+} Magnetic Moment and Internal Field in $SmAl_2$ as Function of Temperature. Admixture of $^6H_{7/2}$ into the ground multiplet is included. CEF splitting 3Δ is taken as 120°K. Temperature dependence of magnetic moment and internal field for (1,1,1) with no admixture is shown (dashed curves) for comparison.

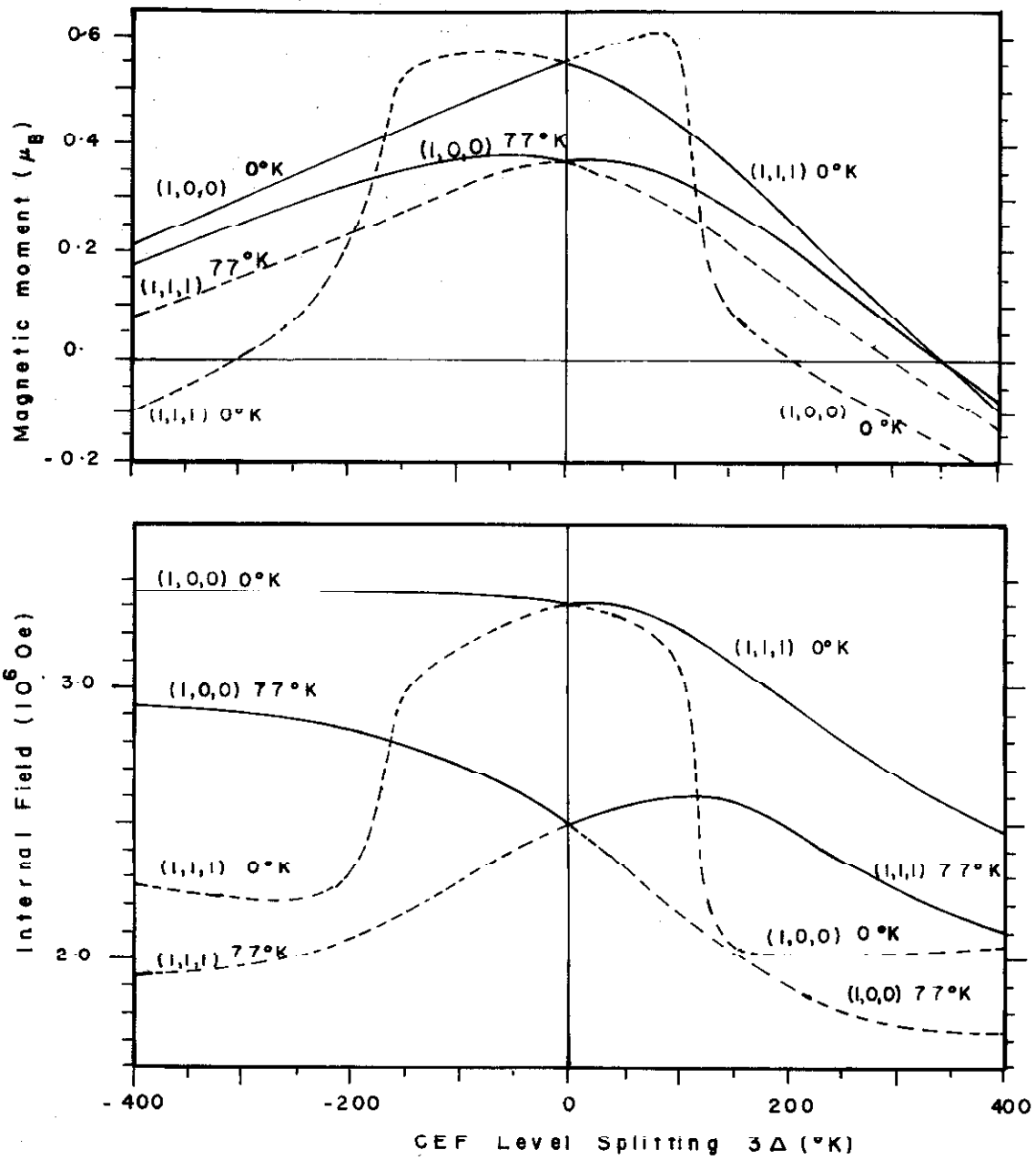

FIGURE IX. Magnetic Moment and Internal Field at $0^{\circ}K$ and $77^{\circ}K$ as a Function of CEF Level Splitting 3Δ with Inclusion of the Admixture of $^6H_{7/2}$ into the Ground Multiplet. - It should be noted that the magnetic interaction energy is not directly proportional to the magnetization or internal field (see Eq. 6). The solid curves give magnetization and internal field for those crystal directions in which the total energy is a minimum (easy axis of magnetization).

as well as on the admixture of the first excited multiplet into the ground multiplet of the ion. In first order perturbation theory, where the admixture is not taken into account, the magnetic moment and internal field are determined by the competition between the crystal field, which tends to decrease these quantities below the free ion values by partially quenching the total angular momentum J, and the exchange, which tends to increase the magnetic moment of the ion and the internal magnetic field at the nucleus by aligning J through its coupling with the spin. In this approximation (Figure VII) the internal field at 0 ^{o}K must be greater than 2500 k0e and the saturation magnetic moment must be greater than 0.55 μ_B per samarium ion, if the crystal field interaction energy is presumed to be less than 400 ^{o}K in magnitude, a value which it is very unlikely to exceed. At 77 ^{o}K the corresponding figures for the internal field and saturation moment for the ion are 2100 k0e and 0.45 Bohr magnetons. In second order perturbation theory, when the admixture of $^{6}H_{7/2}$ into the ground multiplet is included, the contributions of both the crystal field and the exchange to the admixture result in an increased internal field and a decreased saturation moment for the ion. For a crystal field interaction less than 400 ^{o}K, the internal field may be increased by as much as 10%, but spin admixtures into the ground multiplet may in some cases result in a vanishingly small magnetic moment over the whole range of order (Figure IX).

III. EXPERIMENT

A. Recoilless Nuclear Resonance

Recoilless nuclear resonance has, in recent years become, a standard experimental technique of nuclear and solid state physics[37]. In a typical Mossbauer experiment gamma rays from nuclei in a crystalline source are allowed to impinge on a crystalline absorber containing nuclei of the same species, and the transmitted or scattered gamma intensity is recorded as a function of the relative velocity between source and absorber, velocities of the order of a few cm/sec being representative. We take advantage of the high energy resolution of this technique to observe the hyperfine structure of the 22.5 kev gamma transition in Sm^{149}, the details of which are given in Figure I. In the presence of a magnetic field acting at the nucleus, this transition splits into 18 components (Figure X), and the Mossbauer absorption pattern observed is symmetric about its center of gravity if no electric field gradient acts on the quadrupole moments of the nuclear states. In addition, a displacement of the center of gravity of the pattern away from zero velocity may occur. This "isomeric shift" has been discussed by several authors[38, 39].

B. Experimental Technique

The source of gamma radiation is moved with respect to the absorber by an electromechanical vibrator. This velocity spectrometer has been described by Kankeleit[40]. Counts taken through the absorber were stored in successive channels of an RIDL multichannel analyzer operating in multiscalar mode, driven by a stable

Figure X

Position of the 18 components of the Zeeman split 22.5 gamma transition in Sm^{149} as a function of the ratio between the g-factors of the nuclear excited and ground states with the electric field gradient at the nucleus assumed to be zero. The right scale gives the line position in units of the ground state splitting parameter $g_{gr}\mu_N H_{int}$. The left scale gives the velocity at which the line appears if H_{int} is taken to be 3000 kOe. The line AA' marks the value $g_{ex}/g_{gr} = 1.76$ reported by Ofer et al.[43]. Numbers near the lines denote relative intensities.

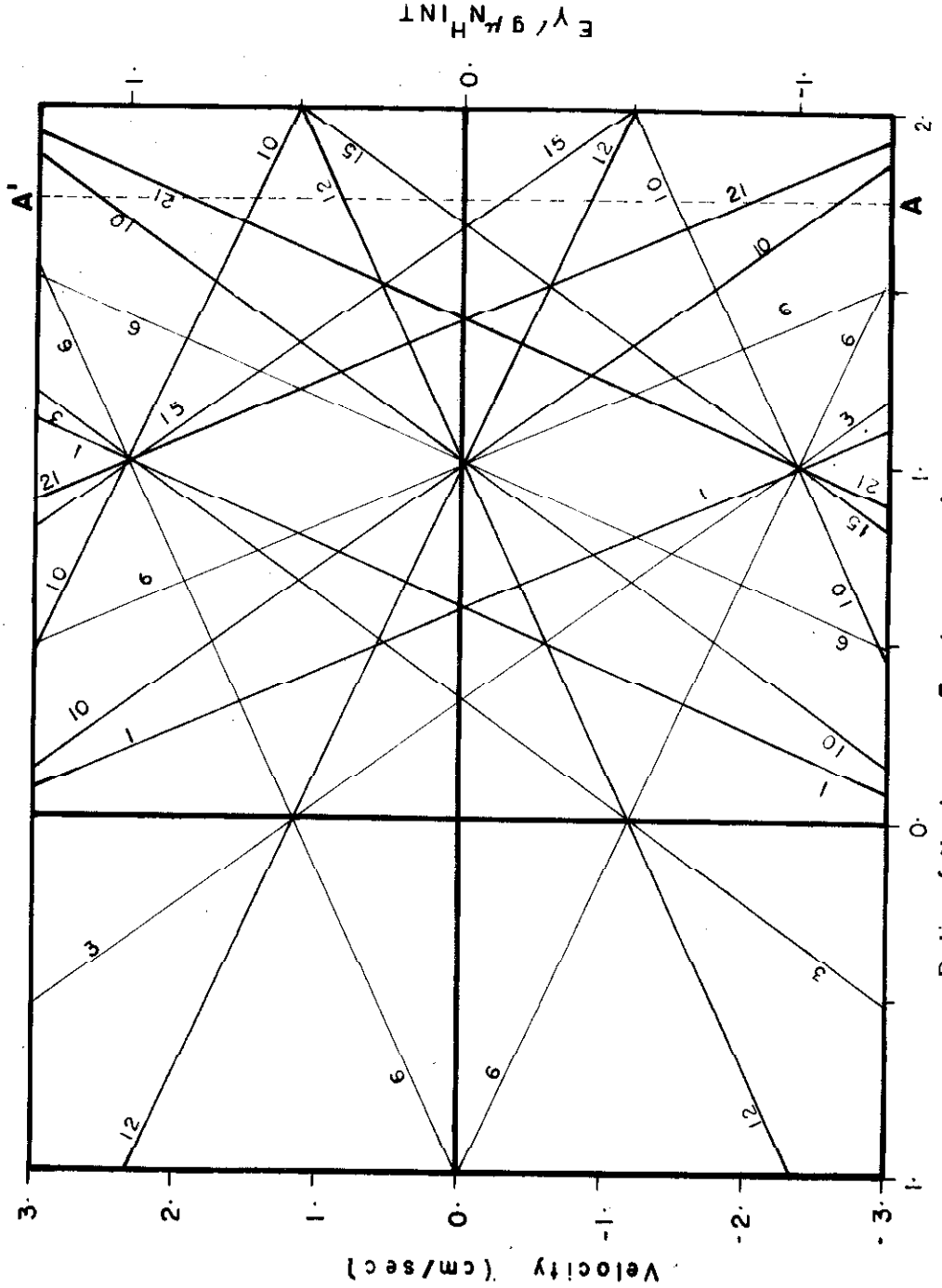
E γ / g μN H INT
A'
A
Velocity (cm/sec)
Ratio of Nuclear g-Factors, g ex / g gr

FIGURE X

crystal oscillator. The driving signal for the vibrator was derived from the kicksorter to ensure synchronism between the velocity wave form and the channel advance, and a feedback system was employed to maintain a triangular velocity wave form. Absolute velocities were determined by calibration against the known nuclear Zeeman splitting of Fe^{57} in iron metal[41].

The source was prepared by proton bombardment of 40 mg of Sm_2O_3 at the Oak Ridge 86 inch 22 Mev cyclotron to produce Eu^{149} by the reaction Sm^{150}(p, 2n) Eu^{149}. The target material was enriched to greater than 90% in Sm^{150}, and an irradiation of 10 hours was performed at a beam current of 60 μa, of which it estimated that 10% was intercepted by the target. The source activity, measured by counting the Sm^{149} 277 kev and 328 kev gamma rays with a thick NaI detector in a well-defined geometry, proved to be on the order of 1/2 mc. The oxide source displayed an unsplit emission line, and it was not found necessary to treat the source further. In Figure XI absorption spectra taken with this source and unsplit absorbers are shown. These lines are 50% broader than the line width $2\Gamma = 1.6$ mm/sec calculated from the reported half-life, 7.6 ± 0.5 ns[42], of the 22 kev level. If this broadening is attributed entirely to the source, then the 22 kev line of Sm^{149} in Sm_2O_3 must be of twice the natural line width, in agreement with the spectra taken of samarium oxide sources against oxide absorbers by Ofer et al.[43]. This broadening of the 22 kev gamma line in the samarium oxide is due to an unresolved quadrupole splitting, most likely.

The weakness of the 22 kev gamma compared with the very strong samarium K X-ray at 39 kev resulting from the preceding electron capture (Figure XII) necessitated the use of a good

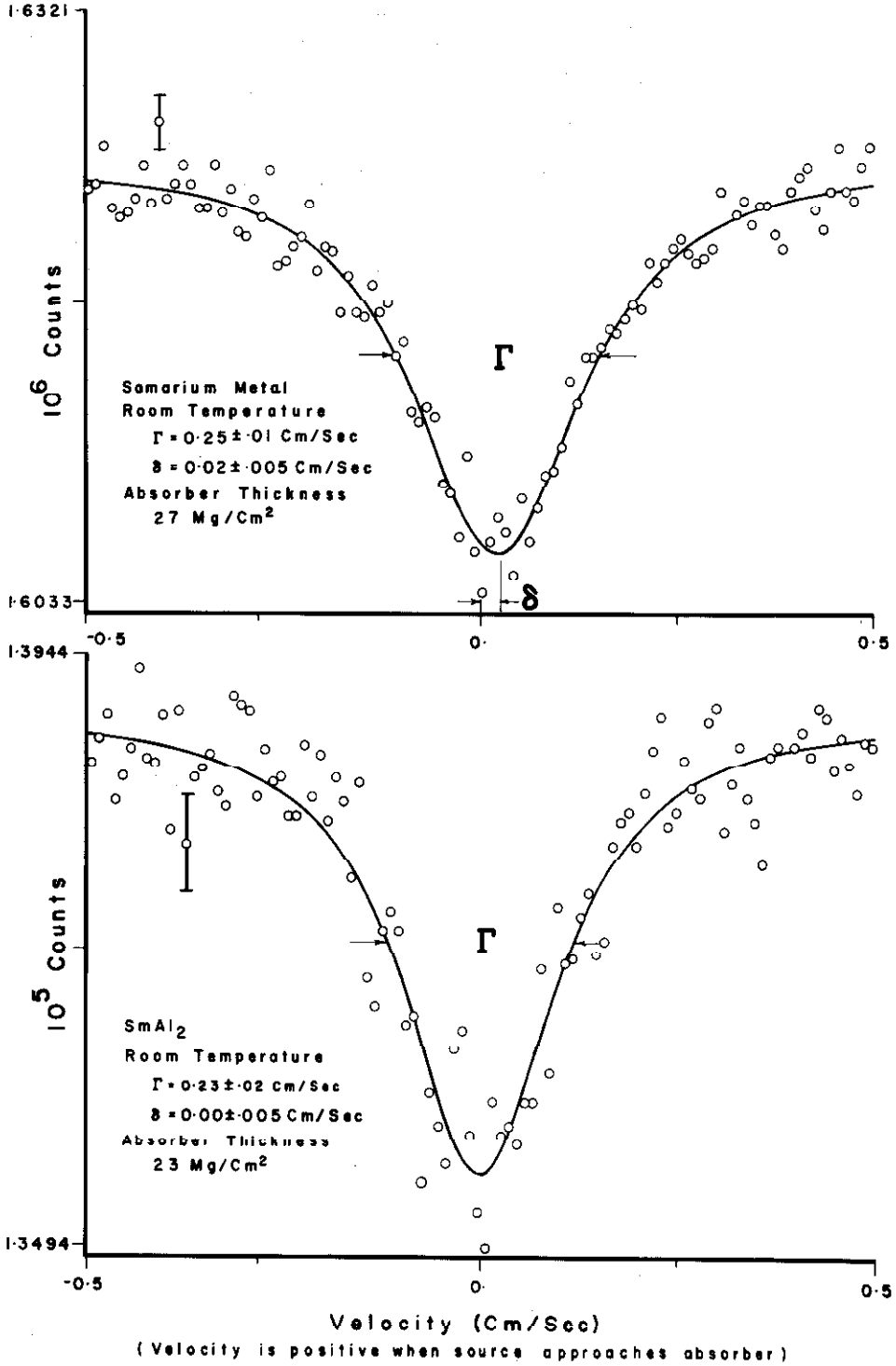

FIGURE XI

Absorption Spectra of the 22·5 Kev Gamma of Sm^{149} Taken with Sm_2O_3 Source and Unsplit Absorbers

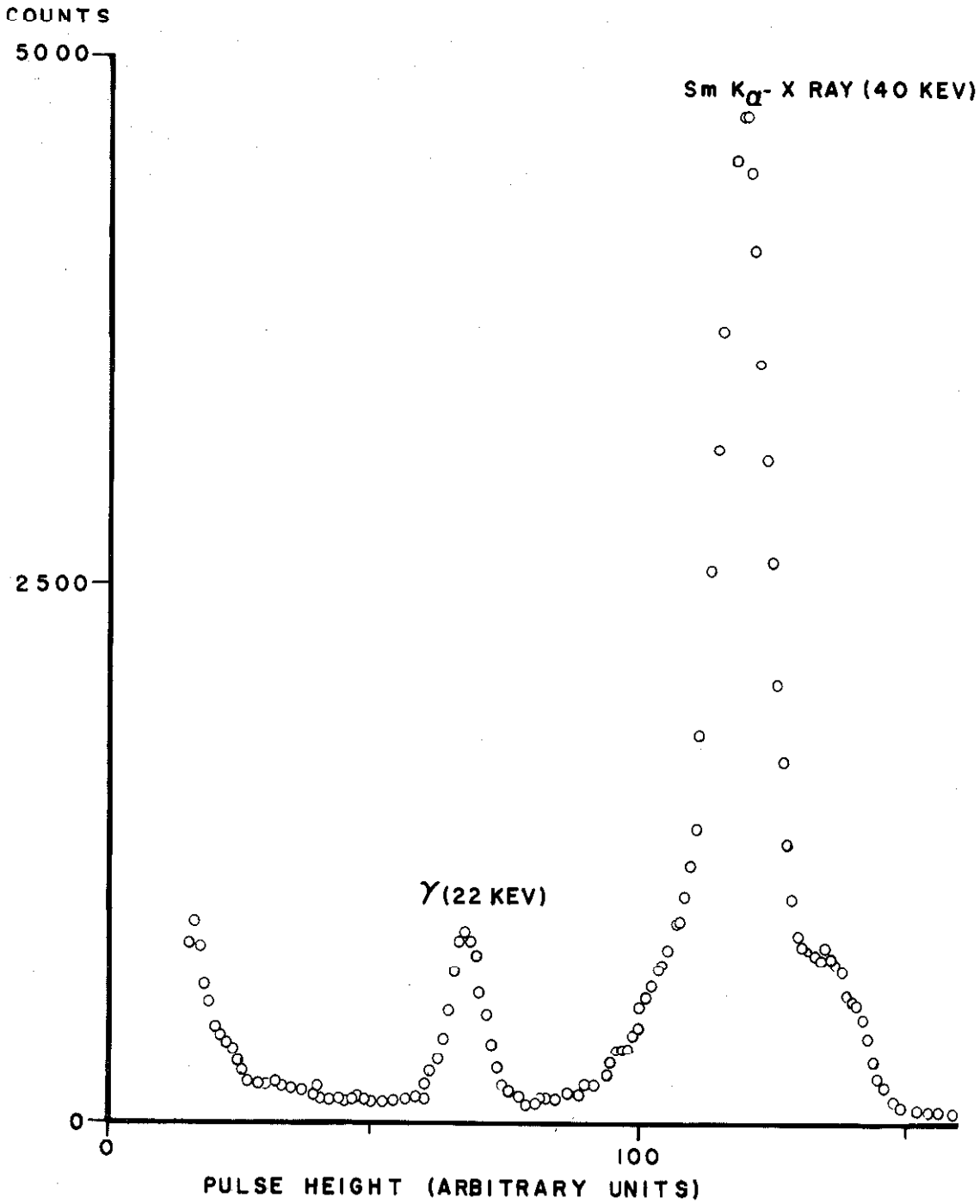

FIGURE XII: Proportional Counter Spectrum of Sm^{149} Taken with 5 atm Argon Counter

resolution gamma detector, and for this reason proportional counters were used. Because of the low activity of the source, a thick counter was required, and an argon- methane filled proportional counter of the type described by Poindexter[44] was mechanically strengthened to allow filling to 5 atm. At this pressure the efficiency of this counter was 22 kev radiation was estimated to be 35%. A commercial xenon-methane filled proportional counter, for which the manufacturer quoted an efficiency of 40% at 22 kev, was also used. These considerations in practice seemed to favor the xenon counter. While the resolutions of the two types of counters were comparable, the actual counting efficiency of the xenon counter seemed to be significantly greater than that of the argon counter.

The $SmAl_2$ was prepared by induction melting of a stoichiometric mixture of 99.99% pure aluminum with 99.9% samarium of the natural isotopic constitution under an argon atmosphere. The structure was confirmed by powder X-ray diffraction analysis. The absorber consisted of 116 mg of the alloy, crushed into a powder, which was passed through a 200 mesh sieve. The powder was rolled into a wax binder and pressed into a one inch diameter disk. The absorber was cooled in a commercial cryostat, described by Snively[45], with provision for continuous variation of the temperature. Resonant absorption spectra were taken at 11 ^{o}K and 77 ^{o}K. At the lower temperature the temperature of the absorber was monitored by measuring the resistance of a precalibrated carbon resistor in good thermal contact with the absorber. At the higher temperature, the temperature of the absorber was measured with a copper-constantan thermocouple, the reference junction of which was cooled in liquid nitrogen.

C. Experimental Results

In $SmAl_2$ at temperatures below the Curie point hyperfine structure is observed in the Mössbauer absorption spectrum. In Figures XIII and XIV, the spectra observed at 77 ^{o}K and 11 ^{o}K, respectively are displayed. In these spectra the nuclear hyperfine structure is not fully resolved, and a numerical fitting procedure is necessary to derive the nuclear hyperfine coupling parameters from the observed spectra. An unexpectedly large nuclear quadrupole coupling is evident from the asymmetry of the spectra, and this coupling is included in the fitting procedure. The observed spectra were fitted with a sum of Lorentzian line shapes according to a least squares procedure. The conditions determining the minimum are nonlinear; these equations were linearized and solved by an iterative procedure with a digital computer. In general, this iterative procedure converged to local minima near the starting parameters, necessitating a search of parameter space for the absolute minimum. An extensive search was carried out over ranges of parameters seeming reasonable, and the best fits resulting are represented in the figures by solid curves passing through the data points. In these fits the ratio of the nuclear excited and ground state moments, and nuclear excited state spin reported by Ofer et al.[43] were used. The internal magnetic field at the nucleus is derived from the nuclear ground state magnetic splitting, using for the ground state magnetic moment of Sm^{149} the mean of the two measurements recalculated by Bleaney[32]. An approximate fit can also be made using different values for the nuclear g-ratio and spin from those reported by Ofer et al., but

Figure XIII

Mössbauer absorption spectrum of Sm^{149} in $SmAl_2$ at 77 ^{o}K taken with a Sm_2O_3 source at room temperature. The solid curve gives the result of a least-squares fit assuming an I = 5/2 excited state.

Parameters of fit: (Standard deviations contain statistical errors only)

Nonresonant background:	2.588×10^6 counts
Effect normalized to a single line:	$1.95 \pm .002\%$
Line width:	$0.33 \pm .04$ cm/sec
Nuclear ground state magnetic splitting parameter ($g_{gr}\mu_N H_{int}$):	$0.405 \pm .036$ cm/sec
Ratio of nuclear g-factors (g_{ex}/g_{gr}):	$1.74 \pm .04$
Ground state electric quadrupole coupling ($e^2qQ_{gr}/4$):	$-0.63 \pm .08$ cm/sec
Excited state electric quadrupole coupling ($e^2qQ_{ex}/4$):	$+0.058 \pm .061$ cm/sec
Isomeric shift:	$-0.032 \pm .011$ cm/sec
Resulting χ^2 (100 data points)	110

The ground state magnetic splitting parameter corresponds to an internal field of 0.52×10^6 0e if the nuclear ground state magnetic moment is taken as 0.648 μ_N, the mean of the values recalculated in reference 32.

FIGURE XIII

Figure XIV

Mössbauer absorption spectrum of Sm^{149} in $SmAl_2$ at $11^{o}K$ taken with a Sm_2O_3 source at room temperature. The solid curve gives the result of a least squares fit assuming an I = 5/2 excited state.

Parameters of fit: (Standard deviations contain statistical errors only)

Nonresonant background:	3.070×10^6 counts
Effect normalized to a single line:	$2.16 \pm .002\%$
Line width:	$0.32 \pm .07$ cm/sec
Nuclear ground state magnetic splitting parameters ($g_{gr}\mu_N H_{int}$):	$1.49 \pm .03$ cm/sec
Ratio of nuclear g-factors (g_{ex}/g_{gr}):	$1.77 \pm .01$
Ground state electric quadrupole coupling ($e^2qQ_{gr}/4$):	$-0.72 \pm .08$ cm/sec
Excited state electric quadrupole coupling ($e^2qQ_{ex}/4$):	$-0.38 \pm .07$ cm/sec
Isomeric shift:	$-0.16 \pm .02$ cm/sec
Resulting χ^2 (100 data points):	150

The ground state magnetic splitting parameter corresponds to an internal field of 1.92×10^6 0e if the nuclear ground state magnetic moment is taken as $0.648\ \mu_N$.

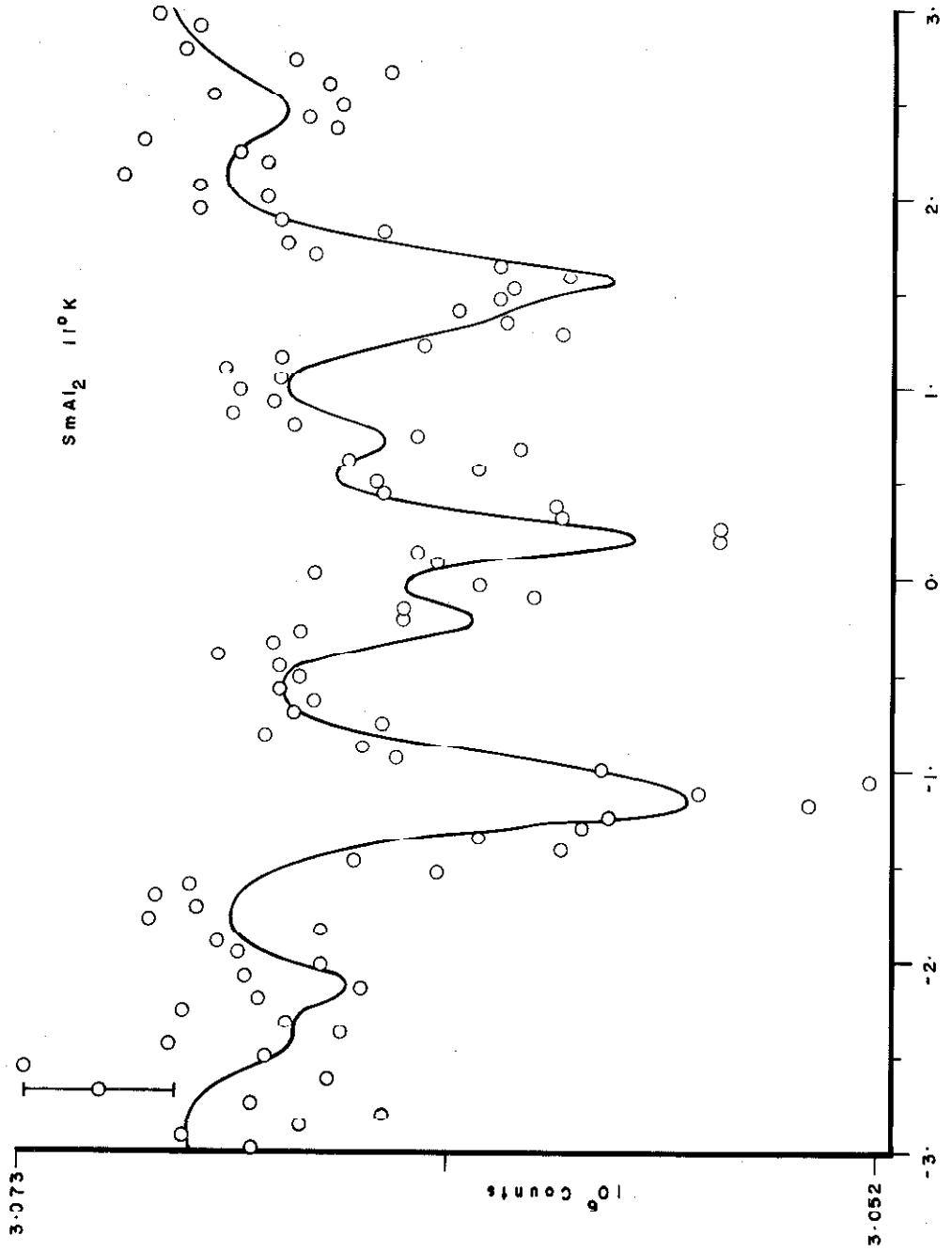

FIGURE XIV

in no case is a better fit obtained than with the parameters listed on the figures. In particular it has not proved possible to fit the spectra using the internal fields predicted on the basis of the crystal field theory discussed earlier. The values of the internal field at 11 ^{o}K and 77 ^{o}K resulting from the best fits to the experimental data are given in Table IX.

Temperature	Minimum Internal Field Resulting From Theory	Experimental Value
(^{o}K)	(0e)	(0e)
11	2.5×10^{6}	1.92×10^{6}
77	2.1×10^{6}	0.520×10^{6}

Table IX

Comparison with experiment of the minimum predicted values of the internal field, assuming a crystal field interaction smaller than 400 ^{o}K in magnitude.

IV. DISCUSSION

In Table IX the values of the internal field at 11^{o} and 77 ^{o}K derived from the best fits made to the observed spectra are compared with the values resulting from the calculation we have made earlier assuming a reasonable size crystal field interaction. There is an evident discrepancy between the values predicted by this theory and the values resulting from experiment. We shall discuss within the framework of the combined molecular field and crystal field theory possible sources of this discrepancy.

i) The size of the crystal field

Our results could be accounted for by assuming a very much larger value of the crystal field interaction than the 400 ^{o}K which is used in Table IX to derive the limits of the values of the internal fields predicted by the theory. This value is already five times larger than that observed in ionic salts of samarium, and it does not seem reasonable to expect a still larger value of the crystal field in metallic samarium compounds where shielding of the ionic charges by the conduction electrons must occur.

We have not considered an admixture of the next higher multiplet by the A_6 terms of the crystal field. Such an admixture might lead to either an increase or a decrease in the internal field, depending on the sign of A_6. A point charge model of the crystal field following White et al.[20] suggests that such an admixture is negligible, but the fit of Bleaney[17] to the specific heat of praesodymium metal leads to a ratio between A_4 and A_6 that would imply an admixture by A_6 comparable to that by A_4. However, although an admixture by the A_6 terms of the crystal field might give

a reduction in the internal field, a reduction large enough to bring agreement between theory and experiment would imply an increase in the magnetic moment of the ion five times larger in magnitude than the reduction in the internal field (the ratio of the reduced matrix elements of the internal field operator, N_1/N, is about five times smaller than, and opposite in sign to, the ratio g_1/g of the reduced matrix elements of the magnetic moment operator). Since a saturation magnetization very much smaller than the free ion values, rather than very much larger, is measured in $SmAl_2$[5] and in other samarium intermetallic compounds[46], we conclude that the neglect of the A_6 terms is not the source of the discrepancy between theory and experiment.

ii) The question of the nuclear spins and magnetic moments

The ground state spin of Sm^{149} has been unambiguously determined by several authors. The presently available measurements of the ground state magnetic moment, however, rest on the study of the magnetic hyperfine interactions in the atom or ion, and the derivation of the magnetic moment from these experiments depends on a knowledge of the electron wave function, particularly the parameter $\langle r^{-3} \rangle_{4f}$. Bleaney[32] has reviewed the data on the hyperfine interactions in the rare earth region, and using recent direct measurements of the magnetic moments of certain isotopes of the rare earth elements, has derived $\langle r^{-3} \rangle_{4f}$ from magnetic resonance experiments on the ions and atoms of these elements, and Bleaney has estimated this parameter for the remainder of the rare earth series by interpolation. The nuclear magnetic moment we have used in this study has been derived by Bleaney from experiment using this interpolated value of $\langle r^{-3} \rangle_{4f}$ and the error estimated by

him is about 2%, mainly arising from the interpolation. Moreover, Bleaney's interpolated value of $\langle r^{-3} \rangle_{4f}$ has been used in the present work to derive the theoretical values of the internal field, and thus the ratio between the theoretical and experimental values of the internal field is not affected by an error in the magnetic moment arising from $\langle r^{-3} \rangle_{4f}$.

The magnetic moment of the Sm^{149} excited state is not well known, nor is its spin. A spin assignment of 7/2 has been reported by Harling et al.[47] on the basis of angular correlation studies. Ofer et al.[43] report a spin assignment of 5/2 on the basis of Mössbauer studies of the Sm^{149} hyperfine interaction in samarium iron garnet. The only value of the excited state magnetic moment reported is that given by Ofer et al. on the basis of their garnet studies. The interpretation of the Mössbauer spectra observed in the garnet is complicated by the presence of a number of magnetically inequivalent sites for the samarium ion in this material, and the data of these authors is not unambiguous. They did not succeed in resolving these spectra into the component lines. The ratio of nuclear g-factors and the spin of the 22 kev nuclear excited state they determine by fitting theoretical spectra to the observed absorption pattern at 16 ^{o}K. In these fits there are definite discrepancies between the theoretical spectra and the observed absorption pattern in the positions of the smaller peaks, which are attributed by the authors to the complicated structure of the material. Figure X would indeed suggest that the three peak pattern we observe in $SmAl_2$ could perhaps be fit with a ratio of unity between the nuclear g-factors. Ofer et al. have considered this possibility in the interpretation of their data, and have rejected it. However, if we assume this value for the ratio of g-factors, the internal field in $SmAl_2$ at

11 ^{o}K must be taken to be about 1500 kOe, which represents an even larger discrepancy between theory and experiment. Indeed we have tried yet other g-factor ratios and other values for the spin of the nuclear excited state and have not succeeded in producing a better fit to the experimental data than that obtained using values of Ofer et al. We nevertheless feel that the values of the nuclear excited state spin and magnetic moment remain an open question.

iii) Core polarization

The contribution to the internal magnetic field at the nucleus made by s electron spin density there, acting through the Fermi contact interaction has thus far been neglected. One such source of s electron spin density is the polarization of the core s electrons of an ion by its own unpaired 4f electron spins. The core polarization contribution to the magnetic hyperfine interaction in the rare earth region has been estimated by Bleaney[32] on the basis of the analysis of Baker and Williams[48] of their ENDOR studies of Eu^{++} in CaF_2, where a magnetic hyperfine interaction corresponding to an internal field of -340 kOe was observed. If pure Russell-Saunders coupling is assumed for Eu^{++}, the ground multiplet is $^{8}S_{7/2}$, and the measured internal field results entirely from core polarization. However, the analysis by Baker and Williams of their data and the atomic beam measurements of the magnetic hyperfine structure in the europium atom indicates that of the field observed in the ion 75% may be assigned to core polarization effects and 25% may be assigned to a field from the 4f electrons arising from a breakdown of Russell-Saunders coupling. Bleaney, in analogy to the trend of the core polarization contribution observed in the iron group ions, suggests that this contribution in the rare earth series

be taken proportional to the spin of the ion, and, on the basis of the europium data suggests a core polarization contribution to the magnetic hyperfine interaction corresponding to

$$H_{int}(\text{core}) = -80\ (g - 1)\langle J_z \rangle \text{k0e} \quad ,$$

where g is the Lande g-factor, and the factor g - 1 arises from the projection of the spin onto the total angular momentum vector J. The europium data indicates that the core polarization is directed oppositely to the spin of the ion in agreement with the analysis of Freeman and Watson[49]. In the case of Sm^{+++}, where the expectation value of the spin operator is increased by admixtures of excited states, it is likely more nearly correct to take

$$H_{int}(\text{core}) = -80\ \langle S_z \rangle \text{k0e} \quad .$$

As the spin is oppositely directed to the internal field in Sm^{+++}, taking into account the core polarization contribution will increase the theoretical predictions by about 4 - 5%.

iv) The question of conduction electron polarization

The second source of net s electron spin density at the nucleus is the polarization of the s conduction electrons by the spins of the ions in the sample. The magnitude of this contribution is difficult to assess. The internal field of 264 k0e found in europium metal by Barrett and Shirley[50] and by Kienle[51], when compared with the 340 k0e measured in the divalent europium ion[48] suggest a conduction electron contribution in europium metal of 80 k0e or 600 k0e, depending on the sign of the field in the metal. Ofer et al.[52]

have found in $DyAl_2$ at 4.2 ^{o}K an internal field consistent with the free ion value, and measurements of the internal field in other heavy rare earth metals and intermetallic compounds lead to internal fields differing by no more than 15% from free ion values[53]. Moreover, in the rare earth intermetallic compounds the conduction electron density at the nucleus may be rather small, for the isomeric shift of the 25 kev gamma transition in Dy^{161} measured by Ofer et al.[52] in $DyAl_2$ indicates that the electron density at the nucleus in this substance is more nearly equal to that in the ionic salt Dy_2O_3 than that in the metal. From these results it seems reasonable to estimate the conduction electron contribution in $SmAl_2$ as 10-15% of the total field, at most. The sign of this contribution is not known. If it is assumed that the conduction electron spin density near the site of an ion is produced mainly by the spin of that ion, then the unrestricted Hartree-Fock calculations of the exchange polarization effect in the free ions of the iron group[54] would suggest that the polarization of the 6s conduction electrons by the unpaired 4f electron spins should produce spin density at the nucleus parallel to the net spin of the 4f electrons. The same conclusions would be drawn from the work of Yosida[24], if simple assumptions are made about the exchange integral between a conduction electron and an electron of the 4f shell. This would in $SmAl_2$ lead to a decrease in the internal field predicted by theory. However, a very recent calculation by Freeman and Watson[55] of the spin density distribution in gadolinium metal shows that, when the conduction electrons and the exchange integral between a conduction electron and a 4f electron are treated more carefully, the magnitude and sign of the spin density at the nucleus is a

sensitive function of the electronic structure of the metal. It is on this basis that we do not believe that a large enough contribution can arise from this source to account for the discrepancy between theory and experiment.

v) The question of the validity of the free ion wave function used

We have not yet considered the effect of a possible breakdown of the Russell-Saunders coupling scheme. Such a breakdown could change the values of the reduced matrix elements (Table Va) appearing in the theory. In fact, Wybourne[56] has performed an intermediate coupling calculation of the multiplet structure of the trivalent samarium ion and has found an admixture of 3 to 4% of ^4G into the two lowest multiplets of the ^6H ground term. However, as both the spin and orbital quantum numbers of this admixed term differ from those of the ground term, the effect of this admixture on the reduced matrix elements of the crystal field, which only involves the spatial variables will be slight. Similarly, the magnetic moment of the ion, and the orbital part of the internal field will be only slightly affected. On the other hand, there may be a quite substantial correction to the magnetic dipole interaction between the 4f electron spin and the nucleus, for calculations carried out by Wybourne[57] to evaluate the effect of intermediate coupling on the hyperfine interaction in the praesodymium atom and in the holmium atom and trivalent ion indicate a correction by a factor of 2 to 3 to this contribution to the internal field. A correction this large in the trivalent samarium ion would produce a 20 to 30% change in the internal field predicted by theory. However, the magnetic moment of the Sm^{149} ground state given by Bleaney[32] was derived from the experimental data under the assumption of Russell-Saunders coupling, and it is to

be expected that if intermediate coupling is taken into account, compensating corrections will be introduced into the theoretical predictions of the internal field and into the internal field derived from experiment with the aid of the Sm^{149} magnetic moment.

vi) Conclusion

We have found it difficult to account for our results within the framework of the combined crystal field and molecular field theory. The molecular field theory has been used with much success in the calculation of magnetization curves[58] and internal fields[59]. However, the validity of applying crystal field theory to metallic substances might be questioned. Indeed it is not obvious to what extent we are justified in speaking of the energy levels of an ion core at all, for it has been suggested by Gossard et al.[60], in order to account for the anomalously large Yb^{171} Knight shift observed in paramagnetic $YbAl_2$, that the 4f levels actually form part of a conduction band. In any case, the conduction electrons must play an important role, and Ofer et al.[52] have suggested that the large field gradients observed in the rare earth iron intermetallic compounds arise from polarization of the closed shells of the ion core by the 3d conduction electrons. Indeed in our case, if the Sm^{149} ground state quadrupole moment of .06 barns determined by Woodgate et al.[61] is accepted, and it is assumed that the quadrupole moment of the excited state is of the same order of magnitude, the field gradient required to fit our data is several times that which would be predicted on the basis of a crystal field model. Comparison of our measurements of the internal field in $SmAl_2$ with the values predicted on the basis of the combined molecular field and crystal

field theory strongly indicates the necessity of including in greater detail conduction electron features into the theory of the internal field. This appears at the moment to be a very difficult task.

REFERENCES

1. J. D. Axe and G. H. Dieke, J. Chem. Phys. 37, 2364 (1962).
2. B. G. Wybourne, J. Chem. Phys. 36, 2301 (1962).
3. J. A. White and J. H. Van Vleck, Phys. Rev. Letters 6, 412 (1961).
4. See O. D. McMasters and K. A. Gschneider, Nuclear Metallurgy Series, (AIME, 1964) Vol. X, p 93 for a list of currently known rare earth intermetallic compounds. See references 5, 33 and 46 below for measurement of the magnetic properties of certain of the Laves phases.
5. H. J. Williams, J. H. Wernick, E. A. Nesbitt and P. C. Sherwood, J. Phys. Soc. (Japan) 17, Suppl. B-1, 91 (1962).
6. W. Low, Paramagnetic Resonance in Solids (Academic Press, New York and London, 1960) p 123.
7. J. H. Wernick and S. Geller, Trans. Metal. Soc. 218, 866 (1960).
8. W. Low, op. cit., p 12.
9. Ibid.
10. Ibid., p 13.
11. B. Bleaney, Proc. Roy. Soc. A276, 28 (1963).
12. W. Low, op. cit., p 32.
13. Ibid., pp 17-27.
14. K. R. Lea, M. J. M. Leask and W. P. Wolf, J. Phys. Chem. Solids 23, 1381 (1960).

15. R. J. Elliott, Phys. Rev. 124, 346 (1960).

16. T. A. Kaplan, Phys. Rev. 124, 329 (1960).

17. B. Bleaney, Proc. Third Conf. on Rare Earth Res. (Gordon and Breach, New York and London, 1964) p 417.

18. B. Bleaney, Proc. Roy. Soc. (London) A276, 39 (1963).

19. B. Bleaney, Proc. Third Conf. on Rare Earth Res., p 499.

20. J. A. White, H. J. Williams, J. H. Wernick and R. C. Sherwood, Phys. Rev. 131, 1039 (1963).

21. K. A. Gschneider, Rare Earth Alloys (Van Nostrand, Princeton, New Jersey, 1961) p 11.

22. M. Ruderman and C. Kittel, Phys. Rev. 96, 99 (1954).

23. T. Kasuya, Prog. Theoret. Phys., 16, 45 (1956).

24. K. Yosida, Phys. Rev. 106, 893 (1957).

25. B. Bleaney, Proc. Roy. Soc. (London) A276, 19 (1963).

26. R. L. White and J. P. Andelin, Phys. Rev. 115, 1435 (1959).

27. A. Messiah, Quantum Mechanics (John Wiley and Sons, New York and London, 1962) p 695.

28. R. J. Elliott and K. W. H. Stevens, Proc. Roy. Soc. (London) A218, 553 (1953).

29. B. R. Judd, Proc. Roy. Soc. (London) A227, 552 (1955).

30. A. Abraham, The Principles of Nuclear Magnetism (Clarendon Press, Oxford, 1961) p 172.

31. R. J. Elliott, Rev. Mod. Phys. 36, 385 (1964).

32. B. Bleaney, Quantum Electronics (Columbia University Press, New York, 1964) p 595.

33. W. E. Wallace and E. A. Skrabek, Proc. Third Conf. on Rare Earth Res., p 431; See also E. A. Skrabek and W. E. Wallace, J. Appl. Phys. 34, 1356 (1963).

34. M. S. Magno and G. H. Dieke, J. Chem. Phys. 37, 2354 (1962).

35. H. Lammermann, Z. Physik 150, 551 (1958).

36. L. D. Landau and E. M. Lifshitz, Quantum Mechanics (Addison-Wesley, Reading, Massachusetts, 1958) p 136.

37. See, for example, Proc. Third International Conf. on the Mössbauer Effect in Rev. Mod. Phys. 36, pp 333-503 (1964).

38. B. D. Josephson, Phys. Rev. Letters 4, 341 (1960).

39. D. A. Shirley, Rev. Mod. Phys. 36, 339 (1964) and references contained therein.

40. E. Kankeleit, Rev. Sci. Instr. 35, 194 (1964).

41. R. S. Preston, S. S. Hanna and J. Heberle, Phys. Rev. 128, 2207 (1962).

42. O. C. Kistner, A. C. Li and S. Monaro, Phys. Rev. 132, 1733 (1963).

43. S. Ofer, E. Segal, I. Nowik, E. R. Bauminger, L. Grodzins, A. J. Freeman and M. Schieber, 137, A627 (1965).

44. J. M. Poindexter, Ph. D. thesis, Department of Physics, California Institute of Technology, Pasadena, 1964.

45. F. T. Snively, Ph. D. thesis, Department of Physics, California Institute of Technology, Pasadena, 1965.

46. R. M. Bozorth, B. T. Matthias, H. Suhl, E. Corenzwit and D. D. Davis, Phys. Rev. 115, 1595 (1959).

47. O. K. Harling, C. A. Ventrice and J. J. Pintrice, Phys. Rev. 132, 807 (1963).

48. J. B. Baker and F. I. B. Williams, Proc. Roy. Soc. (London) A267, 283 (1962).

49. A. J. Freeman and R. E. Watson in The Mössbauer Effect (John Wiley and Sons, New York and London, 1962) p 117. In particular note the physical picture of the situation presented on page 121, bearing in mind that in samarium the unpaired spins, which produce the core polarization, are directed oppositely to the internal field at the nucleus.

50. P. H. Barrett and D. A. Shirley, Phys. Rev. 131, 123 (1963).

51. P. Kienle, Rev. Mod. Phys. 36, 372 (1964).

52. S. Ofer, M. Rakavy, E. Segal and B. Khurgin, Phys. Rev. 138, A241 (1965).

53. Ibid., and references therein.

54. A. J. Freeman and R. E. Watson, op. cit.

55. R. E. Watson and A. J. Freeman, Phys. Rev. Letters 14, 695 (1965).

56. B. G. Wybourne, op. cit.

57. B. G. Wybourne, J. Chem. Phys. 37, 1807 (1962).

58. See, for example, W. P. Wolfe and J. H. Van Vleck, Phys. Rev. 118, 1490 (1960).

59. See, for example, R. L. Cohen, Phys. Rev. 134, A94 (1964).

60. A. C. Gossard, V. Jaccarino and J. H. Wernick, Phys. Rev. 133, A881 (1964).

61. G. Woodgate, F. M. Pichanik and P. G. H. Sanders, unpublished.